

Influence of the Solar Cycle on the North Atlantic Oscillation

Yuhji Kuroda¹, Kunihiko Kodera², Kohei Yoshida³, Seiji Yukimoto⁴, and Lesley J. Gray⁵

¹Meteorological College, Japan Meteorological Agency

²Nagoya University

³Meteorological Research Institute

⁴Meteorological Research Institute

⁵University of Oxford

November 22, 2022

Abstract

We examine the influence of the solar cycle on the North Atlantic Oscillation (NAO) on its pathway from the upper stratosphere to the surface by applying lagged regression analyses to recent observations, historical observations covering 194 years, and an Earth system model simulation covering 165 years. The propagation of the solar signal can well be explained by a top-down mechanism, but one that was strongly affected by ocean dynamics. The solar signal first appears in the subtropical upper stratosphere as a temperature signal. The associated zonal wind signal then propagates downward to the surface in response to stratospheric variability known as the Polar-night Jet Oscillation. The NAO signal tends to appear in February during years of peak solar activity. The solar signal is further modulated such that positive NAO signals tend to appear earlier in winter with increasing years after peak solar activity, which we think to be an oceanic effect. The fluctuations and amplitude modulation of the solar-NAO relationship on a 50-year time scale also suggest that there will be nonlinear interactions between solar forcing and ocean dynamics.

Influence of the Solar Cycle on the North Atlantic Oscillation

Yuhji Kuroda^{1,2}, Kunihiro Koder¹, Kohei Yoshida¹, Seiji Yukimoto¹, and Lesley Gray³

¹Meteorological Research Institute, Tsukuba, Japan

²Meteorological College, Kashiwa, Japan

³University of Oxford, Oxford, UK

Corresponding author: Yuhji Kuroda (kuroda@mri-jma.go.jp)

Key Points:

1. Propagation of the solar signal can be explained by a top-down mechanism strongly affected by ocean dynamics
2. Solar-related NAO signal tends to peak in February of solar maximum years but shows a 50-year scale drift with lagged amplitudes of ~2 years
3. A positive NAO signal tended to appear earlier in winter as the years since peak solar activity increased

Abstract

We examine the influence of the solar cycle on the North Atlantic Oscillation (NAO) on its pathway from the upper stratosphere to the surface by applying lagged regression analyses to recent observations, historical observations covering 194 years, and an Earth system model simulation covering 165 years. The propagation of the solar signal can well be explained by a top-down mechanism, but one that was strongly affected by ocean dynamics. The solar signal first appears in the subtropical upper stratosphere as a temperature signal. The associated zonal wind signal then propagates downward to the surface in response to stratospheric variability known as the Polar-night Jet Oscillation. The NAO signal tends to appear in February during years of peak solar activity. The solar signal is further modulated such that positive NAO signals tend to appear earlier in winter with increasing years after peak solar activity, which we think to be an oceanic effect. The fluctuations and amplitude modulation of the solar-NAO relationship on a 50-year time scale also suggest that there will be nonlinear interactions between solar forcing and ocean dynamics.

33

34 **1. Introduction**

35 Radiative energy from the Sun is the most basic of the sources that drive
36 weather and climate. The discovery of sunspots and their temporal variations led to the
37 belief that solar variation could be an important driving force for weather and climate
38 change. Many observational and simulation studies have investigated the influence of
39 solar variability on weather and climate (e.g., Gray et al., 2010). Examples of recent
40 solar–climate research include studies on upper stratospheric ozone (Dhomse et al.,
41 2016), climate change for a future grand solar minimum (Chiodo et al., 2016; Spiegl &
42 Langematz, 2020), historical changes of the North Atlantic winter climate (Ma et al.,
43 2018), and changes of the Walker circulation (Misios et al., 2019).

44 Satellite observations of the 11-year solar cycle have shown only very small
45 changes ($\sim 0.1\%$) in solar irradiance (Kopp & Lean, 2011), but large changes of 4–8% in
46 the 200–250 nm wavelength range of the ultraviolet (UV) spectrum (Lean et al., 1997).
47 Therefore, there is a well-documented 11-year cycle of the solar-induced temperature
48 signal associated with variations in UV absorption and changes of ozone levels in the
49 stratosphere (Gray et al., 2010). These temperature changes affect the background winds
50 that influence the propagation of planetary waves through their relationship with
51 thermal winds (Kodera & Kuroda, 2002). As a result, the internal mode of variability in
52 the polar night jet is modulated such that the early winter solar signal in the subtropical
53 stratopause triggers the downward propagation of anomalous zonal wind, and an
54 anomalous annular pattern in the sea level pressure (SLP) tends to appear in mid-winter
55 (Kodera, 1995; Kodera & Kuroda, 2002; Kuroda & Kodera, 2002). In the North Atlantic
56 region, it is represented by the modulation of an important mode of climate variability
57 known as the North Atlantic Oscillation (NAO). The climate in North America, Europe,
58 and Eurasia is strongly influenced by the NAO (Hurrell et al., 2003). This process has
59 been well reproduced by simulations with a chemistry–climate model (Matthes et al.,
60 2004, 2006; Mitchell et al., 2015). Thus this “top-down mechanism” plays a crucial role
61 in conveying solar signals to the surface.

62 Recently, however, the role of the ocean in solar–climate interactions has begun
63 to attract attention (e.g., Misios et al., 2019). If this “bottom-up mechanism” (Meehl et
64 al., 2009) is applied to the North Atlantic, the solar signal will be received by the ocean
65 through forcings of the solar-related NAO, but the NAO will also be forced by Sea
66 Surface Temperature (SST), which is controlled by ocean dynamics. Thus, the NAO
67 will be created through the interaction of both of these dynamics. The results of recent
68 numerical experiments conducted with the UK Met Office model have shown that in the

69 North Atlantic region the response of the NAO signal to the oceanic signal is delayed
70 relative to the solar cycle because of the ocean's large thermal inertia (Andrews et al.,
71 2015; Ineson et al., 2011; Scaife et al., 2013), which is consistent with recent analyses
72 using historical observational data (Gray et al., 2013, 2016).

73 However, Chiodo et al. (2019) concluded that NAO-related solar signals since
74 the mid-1960s might have been a chance occurrence due to internal variability and
75 suggested that the model simulations of past solar-climate studies (e.g., Thiéblemont et
76 al., 2015) are either statistically insignificant or absent. This conclusion has important
77 implications for understanding the solar-NAO relationship and needs to be explained in
78 detail. For this reason, we re-examined the relationship by using comprehensive
79 observational data and undertook realistic long-term simulations.

80 This paper is organized as follows. Section 2 describes the data and analytical
81 methods, Section 3 presents the results, which discussed in Section 4.

82

83 **2. Data and Analysis Methods**

84 For recent observational data, we used mainly ERA-Interim reanalysis data
85 from the European Centre for Medium-range Weather Forecasts (Dee et al., 2011) for
86 the period January 1979 to June 2017. Because the reanalysis did not take account of
87 the influence of solar activity, the data tend to be inaccurate in the upper stratosphere in
88 particular, where both the radiative influence of UV radiation and the chemical
89 influence of nitric oxide, which is produced in the mesosphere by incoming solar
90 protons and strongly influences ozone levels (e.g., Bailey et al., 2002), have large
91 impacts. Therefore, we used zonal-mean satellite observation data for atmospheric
92 levels higher than 5 hPa (~37km). Specifically, for our analyses we used satellite data
93 from the US National Centers for Environmental Prediction/Climate Prediction Center
94 (NCEP/CPC, formerly NMC/CAC) for the period January 1979 to June 2007, and
95 November 2008 to June 2017. No satellite data of NCEP/CPC were available for the
96 relatively long period between June 2007 and November 2008; this gap was filled by
97 using bias-corrected Aura-MLS satellite analysis data from the US National Aeronautics
98 and Space Administration (Schwartz et al., 2008). Note that the Aura-MLS reanalysis
99 data were used only to complement the NCEP/CPC satellite data. The satellite data
100 include temperature and geopotential height data, and we calculated zonal wind from
101 the latter by assuming a balanced wind relationship north of 15°N. We calculated
102 monthly zonal-mean values from the daily values provided in the satellite datasets and
103 used only zonal-mean monthly values for the analysis. We made no adjustments to
104 account for the boundary between the satellite data and the ERA-Interim data. We also

105 used the Eliassen–Palm flux (E-P flux) and residual velocities calculated from the ERA-
106 Interim daily data up to 1 hPa to examine the role of dynamical effects on the solar-
107 NAO coupling. For definitions of the E-P flux and residual velocities see, for example,
108 Andrews et al. (1987).

109 Although we consider the above observational data to be accurate and
110 comprehensive, the length of the data record is only about 38 years. Therefore, we also
111 conducted analyses using two reliable historical observational datasets that cover 194
112 years (from 1823 to 2016): a historical station-based NAO index (Jones et al., 1997),
113 and a solar activity dataset based on sunspot numbers. The NAO index was provided by
114 the University of East Anglia Climate Research Unit, UK, and the Sunspot Number
115 (SSN) data were provided by the Royal Observatory of Belgium. To examine SST, we
116 used monthly Extended Reconstructed Sea Surface Temperature version 5 (ERSSTv5)
117 data (Huang et al., 2017) provided by the National Oceanic and Atmospheric
118 Administration (NOAA) for 1854 to 2017. To remove the trend component of the
119 original data, we removed 55-year running averages to provide our basic SST dataset.

120 In addition to the recent and historical observational datasets, we used data
121 from a long-term historical simulation obtained by using the Earth system Model Ver. 2
122 of the Meteorological Research Institute (MRI) of Japan (Yukimoto et al., 2019). This
123 model has four components: atmosphere, ocean, aerosol, and atmospheric chemistry.
124 The atmosphere model has 80 levels in the vertical with the top level at 0.01 hPa, and its
125 horizontal resolution is TL159 (~120 km). The radiation scheme is the same as that in
126 the MRI-CGCM3 model (Yukimoto et al., 2012), and the radiative flux is calculated in
127 9 long-wave bands and 22 short-wave bands that include the visible and UV regions.
128 The simulation was carried out for the period from 1850 to 2014 using the Coupled
129 Model Intercomparison Project Phase 6 (CMIP6) configuration, which takes account of
130 changes in spectral solar irradiance and high-energy particle precipitation (Matthes et
131 al., 2017), historical Earth orbital change, variations in volcanic and other aerosols, and
132 historical changes in greenhouse gas concentrations and land use (see Eyring et al.
133 (2016) for more details). The atmospheric chemistry component calculates ozone
134 concentrations interactively. The Earth system Model can reproduce the equatorial
135 Quasi-Biennial Oscillation (QBO) with a realistic period of about 28 months by using
136 the non-orographic gravity wave parameterization scheme of Hines (1997). After setting
137 atmospheric, well-balanced oceanic, and other initial conditions as described in
138 Yukimoto et al. (2019), a pre-simulation spin-up of 40-years was conducted to allow the
139 oceanic state to reach equilibrium.

140 We performed lagged regression analyses on the recent observations, historical

141 observations, and the long-term simulated historical dataset against proxies for solar
 142 activity. For example, the lagged regression of the i -th spatial grid of SST for the lag of
 143 the k -th year is calculated by

$$144 \quad R(x_i, k) = \left\langle Z(x_i, t_j) \hat{S}(t_{j-k}) \right\rangle_j, \quad (1)$$

145 where $Z(x_i, t_j)$ is the SST at the i -th spatial grid of the j -th year, $\hat{S}(t_{j-k})$ is the
 146 standardized proxy of a solar activity at the $j-k$ -th years, and $\langle \rangle_j$ means averaging over
 147 all the years of j . The statistical significance is evaluated based on the lagged correlation
 148 (Maisel, 1971) defined by

$$149 \quad C(x_i, k) = \left\langle \hat{Z}(x_i, t_j) \hat{S}(t_{j-k}) \right\rangle_j, \quad (2)$$

150 where $\hat{Z}(x_i, t_j)$ is the standardized SST satisfying $\left\langle \hat{Z}(x_i, t_j)^2 \right\rangle_j = 1$ for all x_i .

151 As proxies for solar activity, for the recent observations, we used the annual
 152 mean solar radio flux at 10.7 cm in “solar flux unit” of $10^{-22} \text{ Wm}^{-2} \text{ Hz}^{-1}$ (F10.7 index).
 153 For the historical observations, we used annual mean SSN (dimensionless), and for the
 154 simulated historical data we used the decadal component of total solar irradiance (TSI,
 155 Wm^{-2}). We used different 11-year solar indices for the various datasets because the
 156 F10.7 index can be obtained only from 1947, but it is well-correlated with SSN
 157 measured since 1749. Similarly, because satellite observations show the 11-year
 158 component of TSI to be well correlated with both the F10.7 index and SSN (Gray et al.,
 159 2010), we used the decadal component of TSI for analysis of the simulation.

160 We obtained the decadal component of TSI by first removing 55-year running
 161 averages from the original data to remove prominent 100-year scale trends and
 162 variations, and then calculating annual averages. Note that the 100-year scale trends and
 163 variations exist only for TSI and not for indices used for the observational data. Before
 164 our analyses, we applied the same filtering procedure to all simulated data to remove
 165 low-frequency variability such as the effect of global warming.

166 For the recent observations and model simulation, the NAO was defined as the
 167 leading month-to-month variability of SLP during extended winter (November to April)
 168 for the North Atlantic region from 20° to 70° N and from 90° W to 40° E, following the
 169 definition of Hurrell et al. (2003). The observational data show that the NAO explains
 170 34% of the total variance, far more than the second mode, which explains only 20%.
 171 The spatial pattern we obtained was a typical meridional dipole with its negative center

172 (-7 hPa) over Iceland and its positive center (4 hPa) over the Azores (not shown). The
173 modeled NAO was very similar to that of the observational data except that the positive
174 center over the Azores was 5 hPa (not shown).

175 Because our attention is focused on the variations of the boreal winter
176 associated with the 11-year solar cycle, we used annual mean indices by averaging
177 monthly indices from July of one year to June of the next year. We carried out both
178 simultaneous regression analyses and lagged analyses. For the lagged analyses, we
179 calculated the positive lag by using time-shifted solar index data with the same data
180 length as the data for the simultaneous analyses. To calculate the negative lag, we
181 shortened the data length as necessary because future values of the F10.7 and SSN
182 indices were not available. For the simulated data, however, CMIP6 recommended
183 future TSI data were used without shortening.

184

185 3. Results

186 3.1. Recent Observations

187 In our analyses of recent observational data, we used the observed annual mean
188 F10.7 index data for 1973–2016 (Figure 1). Here, we identify each winter according to
189 the year in which the December of that winter fell (i.e., winter of 2000 means the winter
190 of 2000–2001). The period 1973–2016 includes almost four complete 11-year solar cycles.

191

192

193

194

195

196

197

198

199

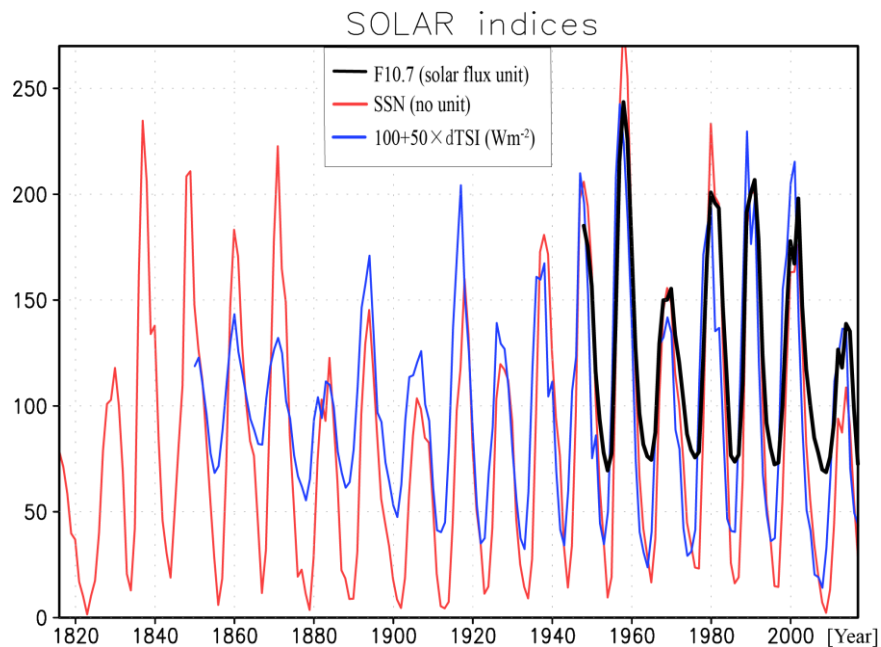
200

201

202

203

204

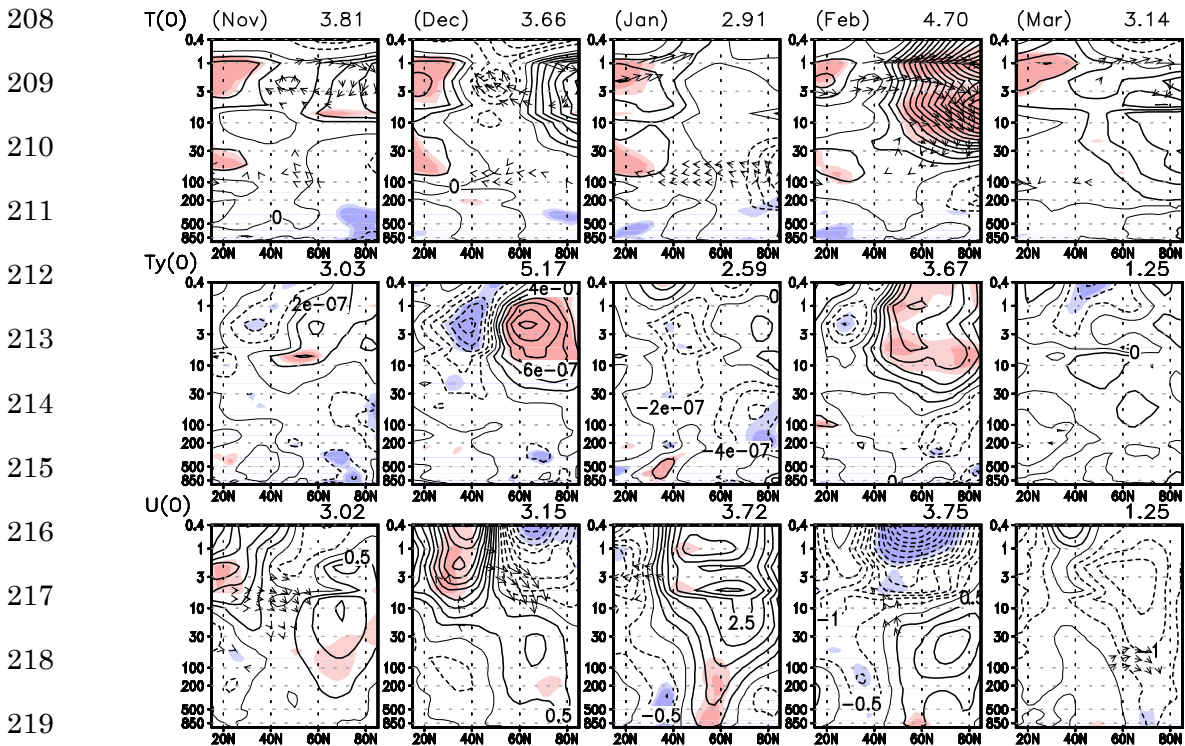


205 Figure 1. Time series of various annual mean solar indices from 1815 to 2016.

206

The regression results for zonal-mean temperature during the northern winter

207 (November–March) against the annual mean F10.7 index with zero lag shows that



220 **Figure 2.** Regressions of observed (upper row) zonal-mean temperature and residual velocities,
 221 (middle row) zonal-mean meridional temperature gradient, and (bottom row) zonal-mean zonal wind
 222 and E-P flux against annual mean F10.7 index from November to March in lag-0 year from 1979 to
 223 2017. The y-axis indicates height (hPa). The x-axis indicates latitude (15°N to 85°N). Light (dark)
 224 shading (red positive, blue negative) indicates areas of greater than 90% (95%) statistical significance.
 225 Only regressions of residual velocities and E-P flux with larger than 95% statistical significance are
 226 shown. Contour intervals are 0.3 K for temperature, 2×10^{-7} K m⁻¹ for the meridional temperature
 227 gradient, and 0.5 m s⁻¹ for zonal wind. E-P flux has been scaled by the reciprocal square root of
 228 pressure. Dashed lines indicate negative values. Numbers annotated above (upper right) each panel
 229 indicate percentage of variance explained by the solar cycle, calculated by areal averaging of squared
 230 correlations.

231 from November to December, regions of higher temperature around the stratopause
 232 tended to appear at latitudes lower than 30°N (Figure 2, upper row). This distribution can
 233 be explained by increased UV radiation according to the climatological latitudinal
 234 distribution of the solar flux during years of high solar activity because UV radiation
 235 directly heats the stratosphere by means of an ozone feedback process (Kodera & Kuroda,
 236 2002; Kuroda & Kodera, 2002). In addition, a temperature minimum in the stratopause
 237 near 50°N and polar heating in the upper stratosphere from November to December were

238 produced by a dynamically driven meridional circulation associated with reduced upward
239 propagation of the E-P flux corresponding to enhanced zonal wind in the upper
240 stratosphere at low latitudes.

241 The zonal-mean temperature profile showed a large negative meridional
242 temperature gradient at around 40°N at the 2 hPa level from November to December
243 (Figure 2, middle panels), although the gradient in November was not statistically
244 significant. There was a positive signal at around 60°N; thus, a meridional dipole structure
245 appeared there from November to December, with the December dipole more significant.
246 Zonal-mean zonal wind signals, which are associated with the meridional temperature
247 gradient in the upper stratosphere (Figure 2, lower panels), can be explained by the
248 thermal wind relationship. In particular, a significant positive wind signal at around 20°N
249 at 1 hPa in November was amplified and shifted to around 30°N and 0.4 hPa in December,
250 although it was less significant in December. This positive anomalous wind signal then
251 shifted poleward and downward in subsequent months until February when it was in the
252 lower polar stratosphere. This poleward and downward movement of the anomalous
253 zonal-mean zonal wind represents natural variability caused by the interaction of
254 planetary waves with the zonal-mean field in the winter stratosphere, which is known as
255 the Polar-night Jet Oscillation (PJO) (Kuroda & Kodera, 2001) and is not directly related
256 to solar activity. However, PJO activity causes the solar signal created in the upper
257 subtropical stratosphere in early winter to move downward during subsequent months.
258 We have proposed this top-down mechanism of solar influence in our previous studies
259 (Kodera & Kuroda, 2002; Kuroda & Kodera, 2002).

260 We next examined the effect of the solar cycle on the SLP in the North Atlantic
261 (Figure 3). We found that a meridional dipole structure characterized by anomalously low
262 (high) SLP tended to build in the northern (southern) part of the North Atlantic from
263 January to February for lags of -1, 0, and +1 years. This pattern is comparable to the
264 pattern associated with the positive phase of the NAO.

265

266

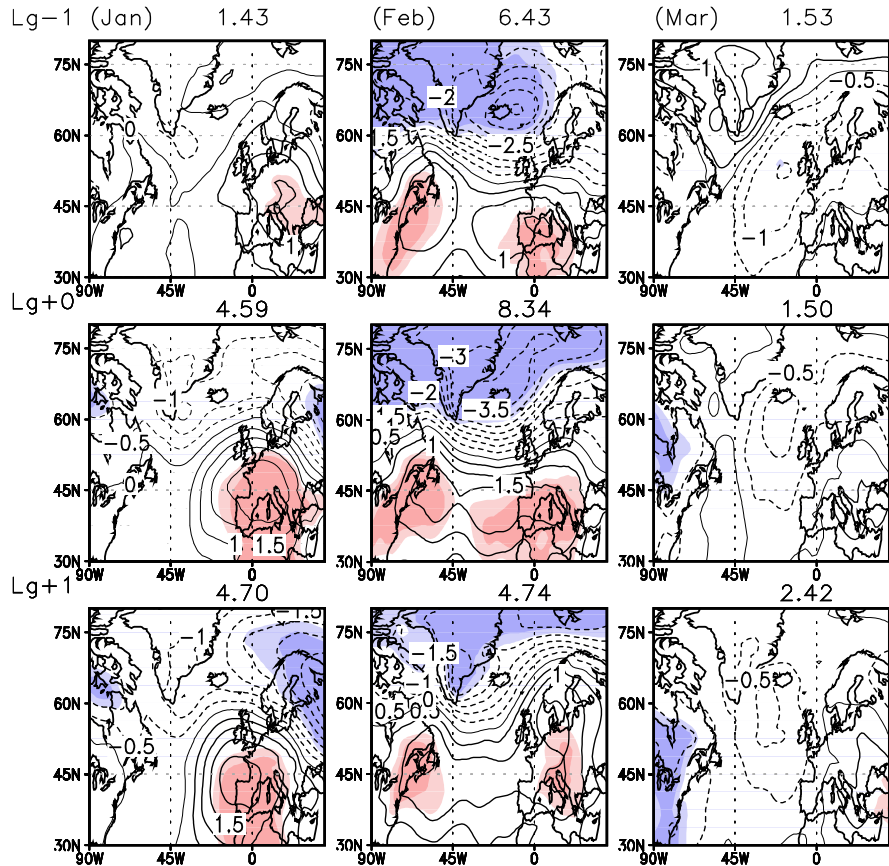
267

268

269

270

271
272
273
274
275
276
277
278
279
280
281
282
283
284
285
286
287



288
289
290
291
292
293
294

Figure 3. Lagged regressions of observed SLP (contour interval 0.5 hPa, negative values shown as dashed lines) against annual mean F10.7 index from January to March (columns) for lag years -1, 0, and +1 (top to bottom) from 1980 to 2017. Dark (light) shading (red, positive values; blue, negative values) indicates areas of greater than 95% (90%) statistical significance. The positive lags correspond to the years when solar activity leads SLP. Numbers annotated above (upper right) each panel indicate the percentage of variance explained by the solar index, calculated by areal averaging of squared correlations.

295
296
297
298
299

To examine the evolution of the PJO during the seasonal march, it is convenient to use PJO space (Kuroda & Kodera, 2004), which is defined by the first two principal components (PC1 and PC2) of the empirical orthogonal functions (EOFs) of anomalous polar temperatures (see Appendix A). Thus, the stratospheric state in the i -th month and the j -th year can be represented by the two-dimensional PJO space

300
301
302

$(P_1(m_i, t_j), P_2(m_i, t_j))$, where $P_1(m_i, t_j)$ and $P_2(m_i, t_j)$ are PC1 and PC2 for the i -th month of the j -th year, respectively. The lagged regression of PC1 against annual mean F10.7 index for the i -th month of lag of k -th year can be calculated by

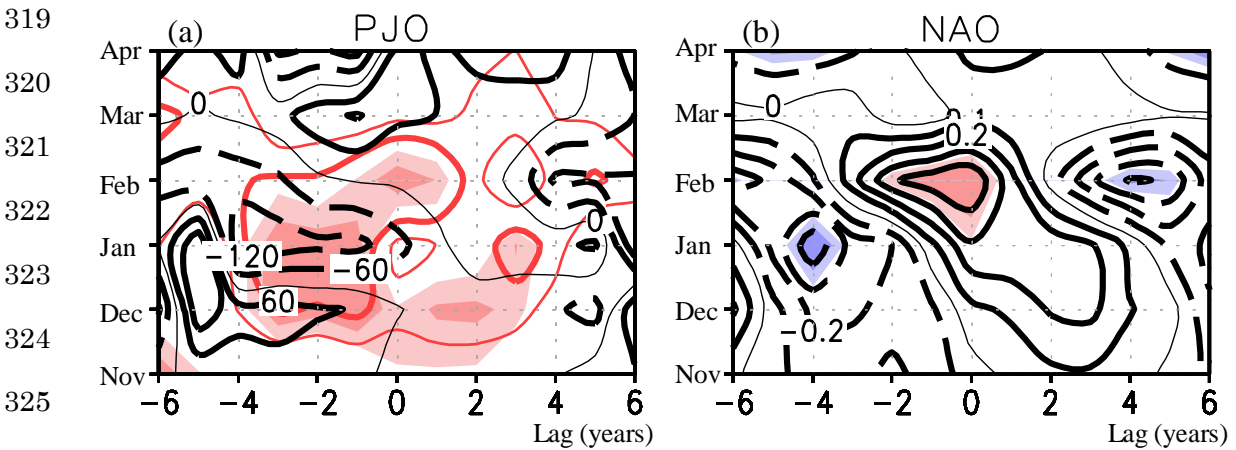
303

$$P1(i, k) = \left\langle P_1(m_i, t_j) \hat{S}(t_{j-k}) \right\rangle_j, \quad (3)$$

304 where $\hat{S}(t_{j-k})$ is the standardized F10.7 index for the $j-k$ -th years, and $\langle \rangle_j$ means
 305 averaging over all the years of j . From these regressions ($P1(i,k), P2(i,k)$), regressed
 306 amplitude $A(i,k)$, and phase angle $\theta(i,k)$ are calculated as

$$307 \quad A = \sqrt{P1^2 + P2^2}, \quad \theta = \tan^{-1} \frac{P2}{P1}. \quad (4)$$

308 Thus, the amplitude $A(i,k)$ is the distance of the regressed state vector from the origin
 309 and the phase angle $\theta(i,k)$ is measured counterclockwise from the positive part of the x
 310 axis (PC1). The statistical significance of PC1 and PC2 can be evaluated from the
 311 correlation with the annual mean F10.7 index. From them the statistical significance of
 312 the amplitude is simply calculated as Eq. (4). Note that phase angles are calculated to be
 313 between -180° and $+180^\circ$. Thus, special attention is needed when there are state vectors
 314 on or near the negative PC1 axis, because they appear as tightly packed contours on either
 315 side of the zero contour (e.g., January at a lag of -4 years in Figure 4a). However, because
 316 we focused mainly on the area around the zero phase angle (i.e., the positive region on
 317 the x axis) which is closely related to the positive NAO during periods of high solar
 318 activity, this was not problematic.



326 **Figure 4.** Lagged regressions of observed (a) PJO indices and (b) NAO index against annual mean
 327 F10.7 index from 1979 to 2017. PJO indices are represented by their amplitudes (red contours) and
 328 phase angles (degrees, black contours). Thick (thin) red contours indicate values of 0.3 (0.2). Dark
 329 (light) shading (red, positive, blue negative) indicates areas of greater than 95% (90%) statistical
 330 significance. Black contours in (a) are at 60° intervals; those in (b) are at 0.1 intervals, and negative
 331 values are shown by dashed lines in both (a) and (b). Thin black line shows zero. Positive lags represent
 332 years when solar activity leads the PJO or the NAO indices.

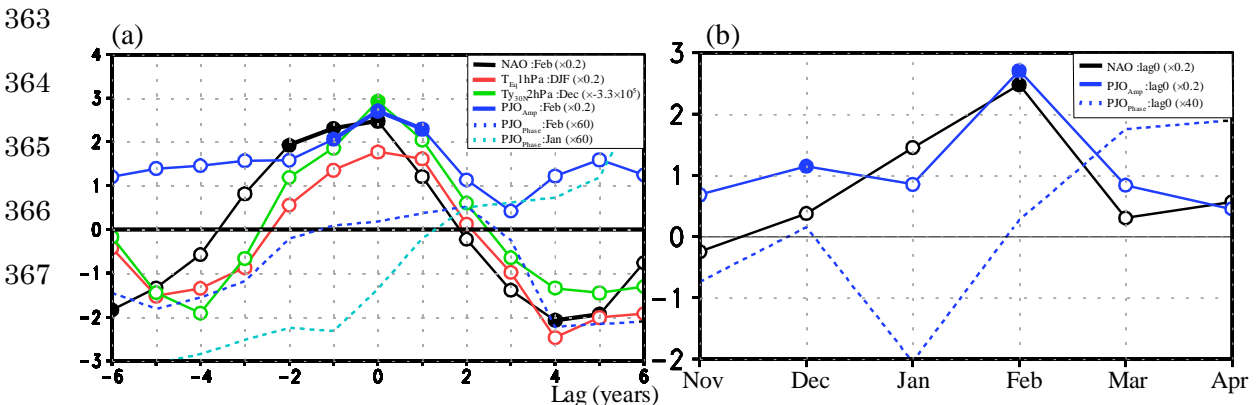
333 The amplitude of the PJO tended to be large from December to February for lags
 334 of -3 to 0 years. During this period, the state vector rotated counterclockwise with the
 335 seasonal march. For example, at the 0 -year lag, the phase angle increased from -60° to
 336 $+60^\circ$ from January to March.

337 Kuroda and Kodera (2004) have shown that, in association with the time
 338 evolution of the PJO, the positive (negative) phase of the Arctic Oscillation, and thus that
 339 of the NAO, tends to appear on the positive (negative) x -axis (PC1). Thus, the positive
 340 phase of the NAO appears at around zero phase angle in PJO space.

341 The lagged regression of the NAO index against the annual mean F10.7 index
 342 (Figure 4b) was consistent with that of the PJO against the solar index (Figure 4a) in that
 343 it showed significantly large positive NAO index values (peak value 0.4) around February
 344 for the 0 -year lag. Note that the standard deviation of the NAO index in February is 1.2 ,
 345 at which time the peak value is rather large. In addition, the peak of the NAO index tended
 346 to appear earlier in winter as the lag in years increased, consistent with the zero phase
 347 angle configuration of the PJO (Figure 4a).

348 To highlight the effect of the pathway of the solar cycle on the NAO more clearly,
 349 we considered the time evolution of key quantities as functions of both the lag of years
 350 and the months of winter (Figure 5). In association with the 11-year solar cycle, both the
 351 December–January–February (DJF)-mean equatorial temperature and the December-
 352 mean subtropical meridional temperature gradient at the stratopause tended to peak at the
 353 0 -year lag. For the same year, the state vector in PJO space tended to intersect the positive
 354 PC1 axis from January to February. The amplitudes of the February-mean PJO index and
 355 the February-mean NAO index also tended to peak at the 0 -year lag (Figure 5a). The close
 356 relationship between the PJO and NAO was also evident in their seasonal evolutions at
 357 their 0 -year lags. In fact, with the seasonal evolution from January to February, the phase
 358 of the PJO increased, and the amplitudes of the PJO and NAO tended to peak in February
 359 when the phase of the PJO approached zero (Figure 5b).

360 Our results thus suggest that these variables vary as a set with the change of the
 361 11-year solar cycle, which is therefore consistent with the previously proposed top-down
 362 mechanism (Kodera & Kuroda, 2002; Kuroda & Kodera, 2002).



368

369

370 **Figure 5.** (a) Lagged regressions of various observed atmospheric quantities against annual mean
371 F10.7 index from 1979 to 2017. Positive lags correspond to years when solar activity leads the other
372 indices. (b) Winter evolution of the NAO-index and PJO-indices regressed against the annual mean
373 F10.7 index at 0-year lag. The values of each atmospheric quantity at each point on its curve can be
374 calculated by multiplying the corresponding value on the y -axis by the number in parentheses in the
375 legend description. The units of measure for equatorial temperature at 1 hPa (T_{eq1hPa}), meridional
376 gradient of temperature at 30°N and 2 hPa ($Ty_{30N2hPa}$), and phase of the PJO index (PJO_{phase}) are K,
377 $K m^{-1}$, and degrees, respectively. On each curve, thick lines and closed circles indicate statistical
378 significance higher than 90%.

379

380 **3.2. Historical Observations**

381 Although there are few parameters for which long-term observational data are
382 available, those that are available can provide very reliable data, in particular, historical
383 station-based NAO index values and solar activity based on SSN. We therefore performed
384 lagged regression analyses of the long-term observational NAO index data, similar to the
385 analyses described above for the recent observational data.

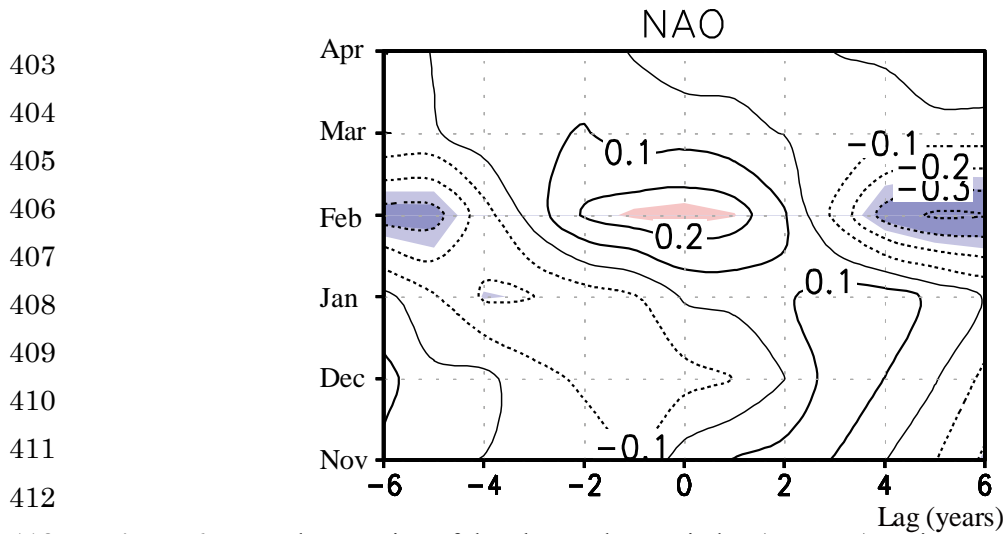
386 The historical station-based NAO index was highly correlated with the EOF-
387 based NAO index described in section 3.1 for the 38 overlapping years (1979–2016); the
388 correlation coefficient (r) of the relationship for the 38 winters (November to April) was
389 0.88, and that for the 38 DJF means was 0.97. Similarly, the historical SSN-based annual-
390 mean solar activity correlated well with the F10.7 index (for 1947–2016, $r = 0.99$).
391 Therefore, comparisons of those observational results with results based on the historical
392 station-based NAO and SSN data will be meaningful.

393 The structure of the solar–NAO relationship based on the 194-year data series
394 (Figure 6) was very similar to that of the solar–NAO relationship for the period from 1973
395 to 2017 (Figure 4b). In both cases, an NAO index peak appeared in February of 0-lag
396 years, and negative peaks appeared in February of lag -5 and $+5$ years. It is noteworthy
397 that the change to a positive NAO index value tended to appear earlier in winter as the
398 lag increased. However, even though the dataset covered a much longer period, the
399 statistical significance of the signals was not very strong.

400

401

402



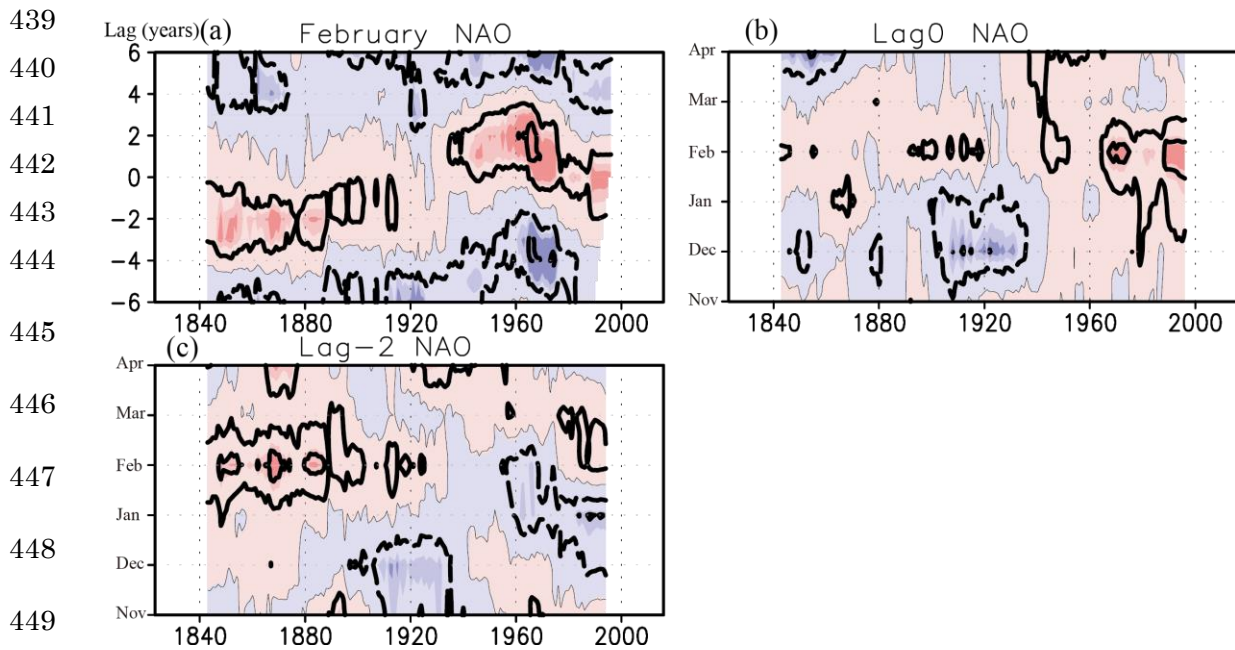
413 **Figure 6.** Lagged regression of the observed NAO index (contours) against annual mean SSN using
414 monthly NAO-index data from 1823 to 2017. The contour interval is 0.1 and negative values are shown
415 by dotted lines. Dark (light) shading indicates areas of higher than 95% (90%) statistical significance.
416 Red (blue) shading indicates positive (negative) values.

417

418 To investigate the temporal changes of the solar–NAO relationship during 1823–
419 2017, we performed lagged regression analyses for running 41-year mean monthly values
420 of the NAO index for each year using a similar approach to that of Ma et al. (2018). The
421 lag years for peak February-mean NAO (Figure 7a) drifted between about –2 and +2 years,
422 and there were large temporal changes in the amplitude of the peak values. For example,
423 the NAO tended to peak at 0.4 around a lag of –2 years for the period centered at 1860
424 and at 0.8 around lags of 1–2 years for the period centered at 1970. In contrast, the
425 amplitude of the peak was very low for the period centered at 1930. However, it is
426 noteworthy that positive NAO signals tended to appear only near lag 0 throughout the
427 entire period analyzed, although the peak showed a 50-year scale drift with an amplitude
428 of about 2 years.

429

430 To see how the month of peaked NAO changed over a longer time scale, we
431 performed similar 41-year regression analyses without lags (Figure 7b). The positive
432 NAO signal appeared predominantly in February without evidence of a decadal drift to
433 other months. However, a decadal change of the signal strength was evident. The signal
434 strength was relatively strong for periods centered at 1840, 1910, 1950, and 1970 and
435 subsequent years, although the signal was significant only for periods centered on years
436 after 1970. However, significant peaks tended to appear in February for lag +1 to +2 years
437 from 1940 to 1980 and for lag –2 years prior to 1920 (Figure 7c). Thus, the existence of
438 a dominantly positive February NAO signal throughout the period 1823–2017 is
noteworthy.



450 **Figure 7.** (a) Lagged regression of the observed February-mean NAO index (contours) against annual
 451 mean SSN data from 1823 to 2017. The x-axis shows the central years for each of the 41-year running
 452 calculations at yearly increments. The shading indicates polarity (red positive, blue negative). The
 453 darkest (middle) shading indicates higher than 95% (90%) statistical significance. The contour interval
 454 is 0.4 and the thin line is the zero contour. (b) Same as (a) but for the lag 0 regression of the NAO
 455 index for each winter month. The contour interval is 0.3 and the thin line is the zero contour. (c) Same
 456 as (b) but for the lag -2 years regression.

457

458 It is well known that the NAO is closely related to the variability of the SST
 459 (Hurrell et al., 2003). Thus, we examined how the SST is influenced by the solar cycle
 460 and how they are both related to the NAO by using the detrended 163-year historical
 461 record of the ERSSTv5 data. Our regression maps for winter (November to April;
 462 Figure 8a to 8c) mean SSTs for lags of 0, 2, and 4 years are similar to those of Kodera et
 463 al. (2016; their Figure 9). At the solar peak year (lag 0), small, positive SST anomalies
 464 (SSTAs) appear only near the east coast of the United States (US) and along the west
 465 coast of Africa. For a lag of 2 years, the positive SSTA near the east coast of the US
 466 extends to the northeast across the Atlantic and reaches a peak of 0.08 K at around 35°N
 467 and 50°W. For a lag of 4 years, the positive SSTA extends farther to the northeast with
 468 its peak reaching 0.09 K at around 45°N and 45°W. Although the shape and amplitude
 469 of this SSTA tend to change with the seasonal march, that change is smaller than the
 470 interannual change and corresponds better to the longer timescale (~1 year) of the SST.

471 Such solar-related SST patterns have some similarity with the so called “NAO

472 SST tripole” pattern, which is obtained by regressing SST against the NAO index
473 (Hurrell et al., 2003). Thus, to simplify our analysis, we have evaluated solar-related
474 NAO changes of the SST by using the index of the NAO SST tripole (called the SST-
475 NAO index). Although both the month-to-month and year-to-year regression patterns
476 show typical tripole patterns, here we used the simpler decadal pattern, which we
477 obtained by regressing low-frequency SST against low-frequency NAO (Figure 8d),
478 both with cutoff frequencies of 8 years. The derived pattern is roughly horseshoe shaped
479 similar to that obtained in the lagged analysis (Hurrell et al., 2003). The monthly SST-
480 NAO index is then defined by projecting the anomalous SST onto the basic pattern for
481 the area from 10°N to 60°N and 80°W to 0°E with standardization.

482 The lagged regression of the SST-NAO index for each month of winter against
483 the annual mean SSN (Figure 8e) shows that the index tends to peak for a lag of 2 years
484 and that the seasonal change is relatively small, although it tends to be stronger in
485 November. The pattern of the lagged regression of the SST-NAO indices for January
486 using running 41-year means of monthly data (Figure 8f) can be regarded as the typical
487 winter pattern because it changes little during the winter months. It is noteworthy that
488 the same calculation for a specific month by treating monthly mean values as annual
489 values gave a similar pattern, probably corresponding to the longer timescale of the SST
490 (not shown). If we compare the solar-related SST-NAO signal with that of the February
491 NAO (green lines in Figure 8f), the former tends to be delayed by 2 to 3 years relative
492 to the latter from 1870 to 1890 and from 1960 to 2000, when solar-synchronous SST
493 signals were more prominent. In fact, the peak of the SST-NAO signal is at lag 3 years,
494 whereas that of the February NAO index is at lag 1 year for 1970. In contrast, the SST-
495 NAO tends to lead by 1 to 2 years from 1940 to 1960, when the NAO amplitude was
496 moderate. However, the SST-NAO was completely out of phase with the February NAO
497 index from 1900 to 1940 when the NAO was weaker. Note that the precedence of the
498 NAO index relative to the SST-NAO index, for example, does not necessarily mean that
499 the NAO alone forces the SST-NAO; rather, their variabilities are mutually sustained for
500 specific lag times, because both indices tend to correlate over a wide range of lag times
501 (Hurrell et al., 2003). Our analysis suggests that there are strong interactions between
502 the solar-related NAO and the SST for relatively long periods, although there are also
503 weaker coupling periods. It is noteworthy that the close relation of solar-related SST to
504 the NAO applies only for the month of February, suggesting that solar-related SST is
505 caused mainly by the top-down mechanism of the NAO.

506
507

508
 509
 510
 511
 512
 513
 514
 515
 516
 517
 518
 519
 520
 521
 522
 523
 524
 525
 526
 527
 528
 529
 530
 531
 532
 533
 534
 535
 536
 537
 538
 539
 540
 541
 542
 543

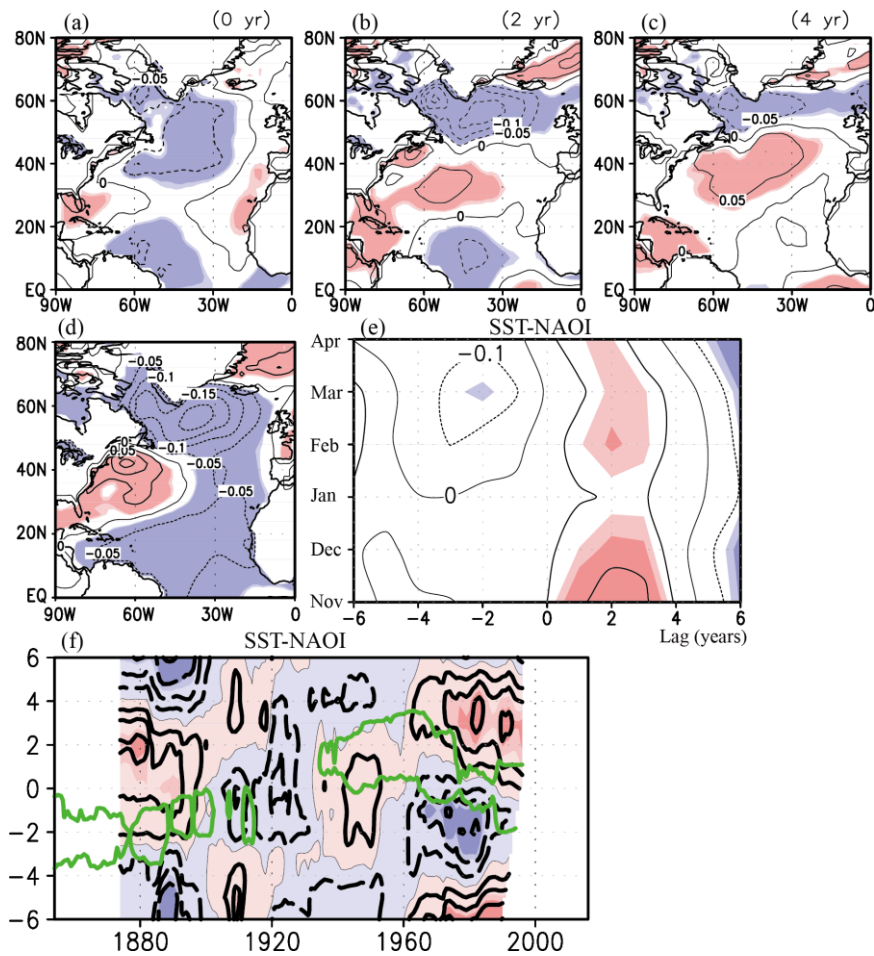


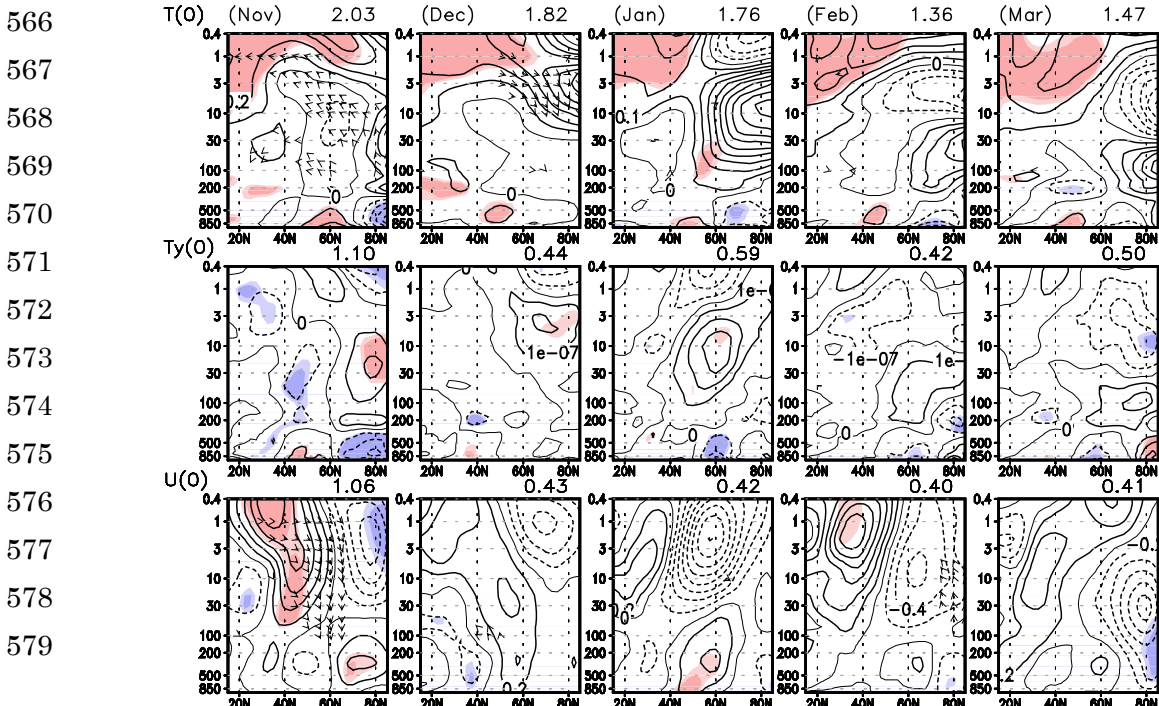
Figure 8. (a)-(c) Lagged regressions (contours) for lags of (a) 0, (b) 2, and (c) 4 years of observed winter-mean SST in the North Atlantic against annual mean SSN from 1854 to 2017. The contour interval is 0.05 K; negative contours are shown as dashed lines. Red and blue shading indicate positive and negative values, respectively. Areas of darker (lighter) shading indicate statistical significance higher than 95% (90%). (d) Same as panel (a), but showing the regression (contours) of the low-frequency component ($T > 8$ years) of SST against the low-frequency component ($T > 8$ years) of the NAO. (e) Same as panel (a), but showing the lagged regression of the SST-NAO index (contours) against annual mean SSN using monthly SST-NAO data from 1854 to 2017. The contour interval is 0.1. The x -axis shows lag years; a positive lag means SSN leads SST-NAO. (f) Lagged regression of the January low-frequency component of the SST-NAO index (contours) against monthly SSN data from 1854 to 2017. The x -axis shows the central years for each of the 41-year running means at yearly increments. The y -axis shows the lag years. The contour interval is 0.1. Red and blue shading indicates positive and negative values, respectively. Areas of darker (lighter) shading indicate statistical significance higher than 95% (90%). The green contours show the same regression for the value of 0.4, but using the NAO index for February.

544

545 3.3 Simulated 1850–2014 data

546 We also performed a lagged regression analysis for the period from 1850 to 2014
547 using data simulated by the MRI Earth system Model. For this analysis we used the
548 standardized decadal component of total solar irradiance (dTSI) as a proxy for solar
549 activity, which is correlated with the other solar indices in the observational data (Gray et
550 al., 2010). Because raw TSI data include a component of a low-frequency, long-term trend,
551 we extracted the decadal component by removing low-frequency variability. Comparison
552 of the scaled dTSI index time series ($= 100 + 50 \times \text{dTSI}$; blue line in Figure 1) with other
553 solar indices used in this study showed that the phase of the dTSI index matched the other
554 indices well, although the amplitude of the dTSI index appeared to show an overall
555 gradual increase after the 1850s. For the regression analysis, we used the same time filter
556 that was used to construct the dTSI index to remove the low-frequency, long-term trends
557 from the modeled data.

558 The lag-0 regression results (Figure 9) showed that a significant temperature
559 signal at the subtropical stratopause tended to appear throughout the winter, as was the
560 case for the observed data. Significantly anomalous westerly winds in the subtropical
561 upper stratosphere in November appeared to be associated with this signal, which
562 subsequently extended downward then moved poleward and created anomalous
563 westerlies around 50°N of the lower troposphere in December and January. Thus, the MRI
564 model produced the downward propagation of the solar signal associated with the PJO
565 well, though it was faster and less prominent than in the observational data (1979-2017).



580

581

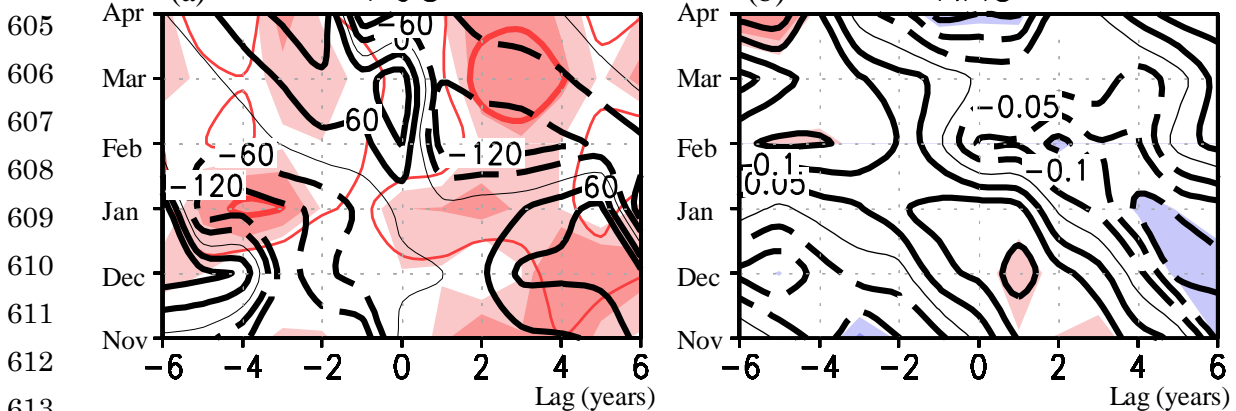
582

583 **Figure 9.** Regressions of simulated (upper panels) zonal-mean temperature and residual velocities,
584 (middle panels) meridional gradient of temperature, and (lower panels) zonal-mean zonal wind and E-
585 P flux against annual mean decadal TSI from November to March for lag 0 year from 1850 to 2014.
586 The y -axis indicates height (hPa). The x -axis indicates latitude (15°N to 85°N). Light (dark) shading
587 (red positive, blue negative) indicates areas of greater than 90% (95%) statistical significance. Only
588 regressions of residual velocities and E-P flux with larger than 95% statistical significance are shown.
589 Contour intervals are 0.1 K for temperature, $1 \times 10^{-7}\text{ K m}^{-1}$ for meridional temperature gradient, and
590 0.2 m s^{-1} for zonal wind. E-P flux has been scaled by the reciprocal square root of pressure. Dashed
591 lines indicate negative values. Numbers annotated above (upper right) each panel indicate the
592 percentage of values explained by the solar cycle, calculated by areal averaging of squared correlations.

593 The lagged results for regression of the PJO against the dTSI index (Figure 10a),
594 where the PJO was defined on the basis of anomalous polar temperatures (see Appendix
595 A), showed the modeled EOF1 (EOF2) to be very similar to the EOF2 (EOF1) obtained
596 for the observed data. Therefore, we defined PJO space by using PC2 as the x -axis and
597 PC1 as the y -axis, with phase angle again measured counterclockwise from the positive
598 region of the x -axis. Together, EOF1 and EOF2 explain almost 95% of the variance of
599 anomalous polar temperatures; thus, the use of PJO space in our analysis is justified.

600 During December to March at lags of around -4 to 0 years, the simulated phase
601 angle structure was somewhat similar to that obtained from the observational data; the
602 phase tended to increase from lower left to upper right (Figure 4a). However, the
603 amplitude tended to be lower, especially in January at a lag of around -1 year.

604



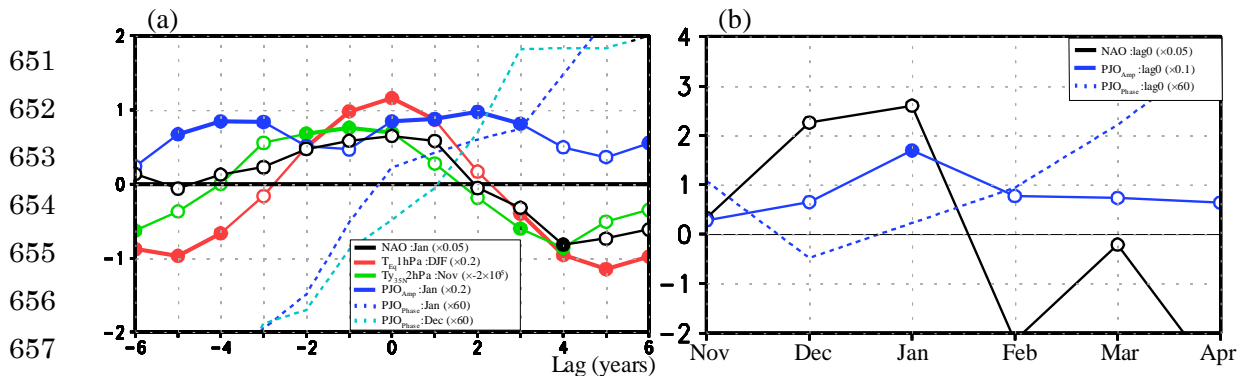
614 **Figure 10.** Lagged regressions of simulated (a) PJO indices and (b) the NAO index against annual
615 mean dTSI index from 1850 to 2014. The PJO indices are represented by their amplitude (red contours)

616 and phase angle (degrees, black contours). Thick (thin) red contours indicate 0.2 (0.1). Dark (light)
617 shading (pink, positive values; blue, negative values) indicates areas of greater than 90% (80%)
618 statistical significance. Black contours in (a) are at 60° intervals; those in (b) are at 0.1 intervals with
619 negative values shown as dashed contours. Positive lags represent years when solar activity leads.
620

621 Consistent with the PJO–dTSI index relationship (Figure 10a), the regression of
622 the NAO index against the dTSI index (Figure 10b) showed an area of positive NAO
623 index around the zero phase angle contour. However, the simulated NAO index values
624 and their statistical significance were much smaller than those obtained from the
625 observation data, despite the much greater temporal extent of the dataset. Thus, we should
626 rely more on the existence of coherent or meaningful structures in the regressed pattern
627 rather than local strength of the statistical significance. It is noteworthy that the positive
628 NAO signal appeared earlier in winter as the number of lag years increased, as was the
629 case for both the recent and historical observational data sets. The positive NAO signal
630 appeared one to two months earlier in the simulated data, although this may be a result of
631 model bias. Note that this bias is common for many CMIP5 models (see Fig. 7 of Mitchell
632 et al., 2015)

633 We next considered the effect of the solar cycle on the NAO in terms of the time
634 evolution of key atmospheric quantities as a function of lag years and its evolution during
635 the winter months (Figure 11). In association with the 11-year solar cycle, both the DJF-
636 mean temperature at the equatorial stratopause and the November-mean subtropical
637 meridional temperature gradient at the stratopause tended to peak at lags of 0 or -1 years.
638 At the 0-year lag, the state vector in PJO space tended to intersect the positive PC1 axis
639 from December to January, and the amplitude of the January-mean NAO index tended to
640 peak, although the amplitude of the PJO index continued to increase until the 2-year lag
641 (Figure 11a). The seasonal evolution of the PJO and the NAO indices for 0-lag years
642 showed that the amplitudes of both tended to increase until they peaked in January (Figure
643 11b). Note also that the phase angle of the PJO intersected zero in January.

644 Note that the PJO indices, which are based on December or January (rather than
645 January or February) means, are shown in Figure 11a because the timing of the downward
646 movement of the modeled PJO tended to be earlier than that of the observational data. We
647 consider this to reflect a model bias. In addition, the tendency of all of the regressed values
648 to be very small reflects the much weaker correlation between these parameters and the
649 dTSI index.
650



651
652
653
654
655
656
657
658 **Figure 11.** (a) Lagged regression of various simulated atmospheric quantities against annual mean
659 dTSI index from 1850 to 2014. Positive lags correspond to years when solar activity leads the dTSI
660 index. (b) Winter evolution of the NAO-index and PJO-indices regressed against annual mean dTSI
661 index at 0-year lag. The values of atmospheric quantity at each point on its curve can be calculated by
662 multiplying the corresponding value on the y-axis by the number in parentheses in the legend
663 description. The units of measure for equatorial temperature at 1 hPa (T_{eq} 1hPa), meridional gradient
664 of temperature at 35°N and 2 hPa (Ty_{35N} 2hPa), and phase of the PJO index (PJO_{phase}) are K, $K\ m^{-1}$,
665 and degrees, respectively. On each curve, thick lines and closed circles indicate statistical significance
666 higher than 80%.

667

668 To examine long-term changes in the solar–NAO relationship, 41-year running
669 lagged regression of the December–January (DJ) mean NAO index is calculated in Figure
670 12a. Our examination (Figure 12a) showed that the peak of the NAO signal tended to drift
671 slowly between lags of about -2 and $+2$ years (Figure 12a). It was at a lag of about -2
672 years for the period centered at 1890, shifted to a lag of about $+2$ years for the period
673 centered at about 1930, and remained at $+2$ until about 1950, after which it drifted slowly
674 to a lag of about 0 for the period centered at about 1970. The amplitude of the NAO was
675 highest around 1890, but by about 1970 it was lower and remained low thereafter.

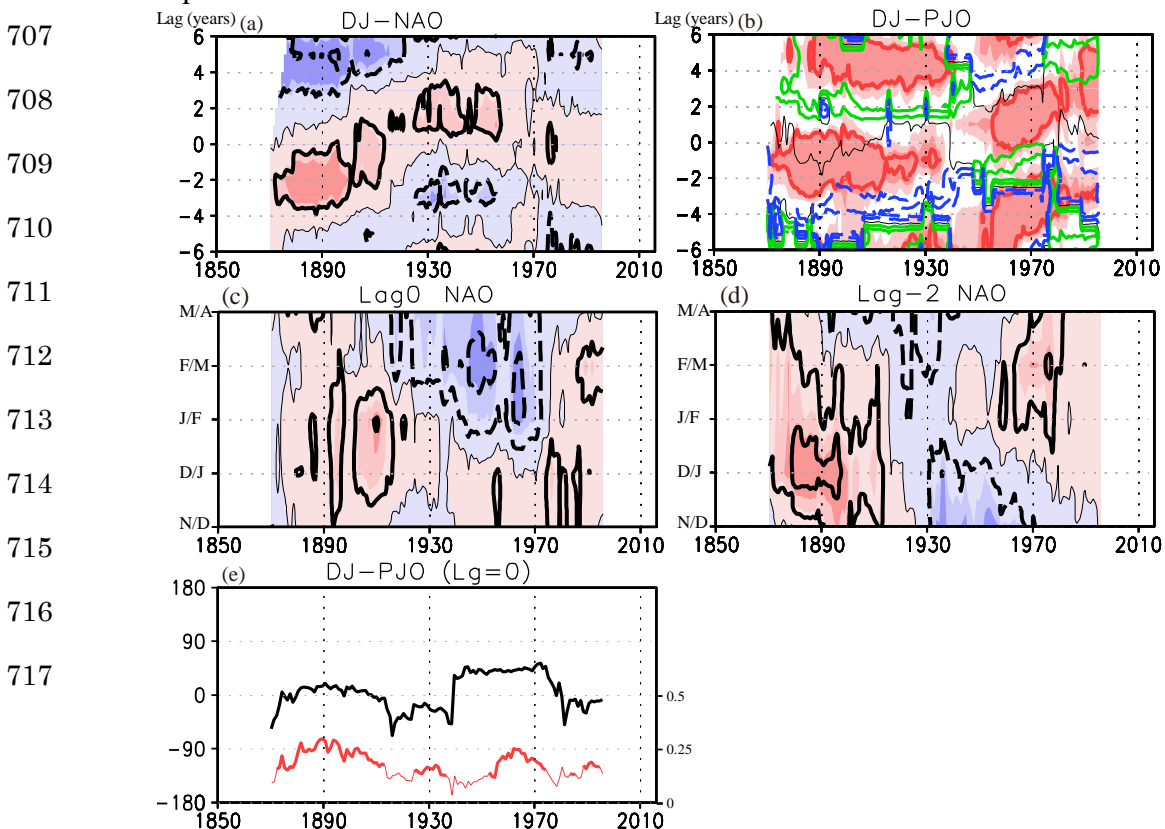
676 To examine the time of appearance of the NAO signal in winter and its longer
677 term changes, we ran the above regressions without lag for two-winter-month periods
678 (Figure 12c). This analysis showed that the NAO signal tended to appear in December–
679 January throughout the period analyzed and to have its highest positive amplitudes for
680 periods centered around 1900 and 1980.

681 Kuroda and Kodera (2004) have shown that NAO signals are strongly affected
682 by the PJO. To examine long-term variations of the PJO, we therefore ran the same
683 regression to the regression in Figure 12a, but for December–January mean PJO indices
684 (Figure 12b). This analysis showed that the zero phase angle of the PJO tended to lie
685 around 0-lag years, but with small shifts between lags of -2 and $+2$ years throughout the

686 period analyzed. The amplitude of the PJO was higher around lags of -1 and $+4$ years
 687 until around 1930, but decreased in amplitude during the period 1930–1950. After 1950,
 688 PJO amplitudes tended to be higher and moved gradually as the years passed to positive
 689 lag years.

690 We also examined the longer term changes of PJO indices by running the same
 691 regression as above but for the December–January mean variation of phase angle for 0-
 692 lag years (Figure 12e). This analysis showed that the phase angle stayed within $\pm 50^\circ$
 693 throughout the period. Kuroda and Kodera (2004) have reported that the positive NAO
 694 tends to appear around the zero phase angle of the PJO, which is consistent with our result
 695 (Figure 12c). Note also that the NAO peaks around 1890 and lag of -2 years (Figure 12d).
 696 Thus, the positive NAO tended to be dominant in December–January throughout the
 697 entire 1850–2013 period.

698 Our results show that the appearance of the NAO tended to be closely related to
 699 the PJO and is thus an indication of stratosphere–troposphere coupling. The persistence
 700 of the near-zero phase angle for the December–January mean PJO around 0-lag years
 701 throughout 1850–2013 suggests strong monthly dependence of the solar cycle on the PJO,
 702 although the modeled progression of the PJO is somewhat faster than that indicated by
 703 the observed data (cf. Figures 5b and 11b). Thus, the long-term variation of the NAO
 704 appears to be influenced not by the PJO alone, but will be also strongly affected by ocean
 705 dynamics. The 50-year scale drift of the December–January mean NAO will be a
 706 consequence of oceanic influence.



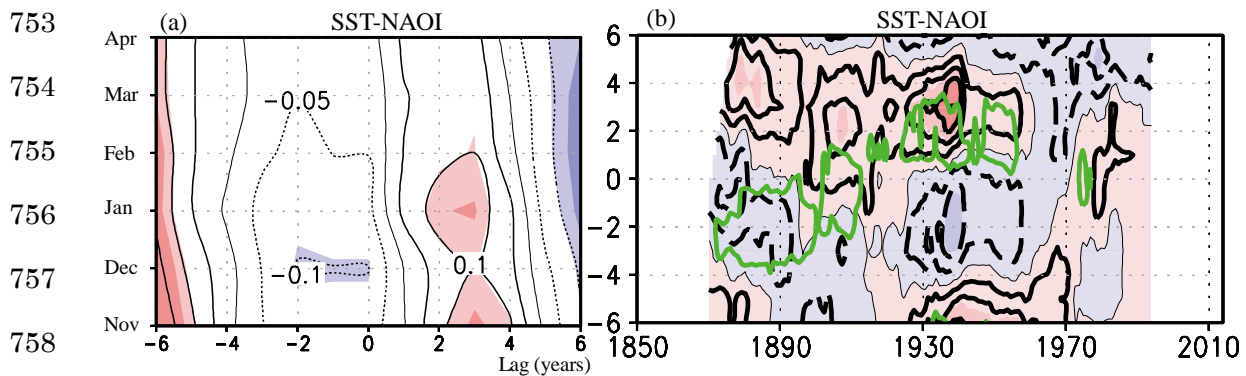
718

719

720 **Figure 12.** (a) 41-year running lagged regression of the simulated December–January (DJ)-mean NAO
721 index (contours) against annual mean dTSI data from 1850 to 2013. The x -axis shows the central years
722 for each of the 41-year running calculations at yearly increments. The shading indicates polarity (red
723 positive, blue negative). The darkest (middle) shading indicates greater than 90% (80%) statistical
724 significance. The contour interval is 0.2 and the thin line is the zero contour. (b) Same as (a) but for
725 DJ-mean PJO indices. The thick red contour is amplitude 0.2, and the shading indicates statistical
726 significance for the PJO amplitudes. The colored contours are phase angle (interval 60°). The thin
727 black line is the zero phase-angle contour and the solid green (dashed blue) line indicates positive
728 (negative) values. (c) Same as (a) but for the lag 0 regression of the NAO index for two-winter-month
729 periods. The contour interval is 0.15 and the thin line is the zero contour. (d) Same as (a) but for the
730 lag -2 regression of the NAO index for two-winter-month periods. (e) DJ-mean phase angle (black,
731 degrees) and amplitude (red, right-hand labels) of the PJO at 0-lag years. Positive lags indicate years
732 when solar activity leads. Thick red lines indicate statistical significance higher than 80 %.

733

734 Thus, we examined lagged regressions of solar-related SST and compared them
735 to those of the historical observation data. For this purpose, we defined the SST-NAO
736 index in the same way as in the historical observations, but excluding the area from
737 45°N to 60°N and 80°W to 45°E , where SST showed large variability. The lagged
738 regression of monthly SST-NAO index against the dTSI index (Figure 13a) shows the
739 SST-NAO peak signal at lags of about +3 and –6 years and that the seasonal variation of
740 the solar signal is small, although it tends to be stronger in early winter. It is noteworthy
741 that for positive lag years the overall pattern is very similar to that of the observation
742 data (Figure 8e). The 41-year running mean lagged regression of the SST-NAO index
743 for January using all monthly data (Figure 13b) produced very similar signals to those
744 of each winter month if the same calculations are performed by treating monthly mean
745 values as annual values. From about 1900 to 1960 (when the solar-related signal was
746 stronger), the SST-NAO tended to lag the DJ-NAO index (green lines in Figure 13b) by
747 1 to 3 years. In fact, the peak of the SST-NAO index was at lag 3 years, whereas the
748 peak for the DJ-NAO index was at lags of 1 to 2 years around 1940. Note that the larger
749 amplitude of the SST-NAO index around 1940 corresponds to largest lag of the DJ-
750 NAO index. The close relation of these signals suggests a close relation between solar-
751 forced NAO and SST. The resemblance of the solar-related SST-NAO signal to that of
752 the DJ-NAO index also supports this relationship.



759 **Figure 13.** (a) Lagged regression of the simulated SST-NAO index (contours) against the dTSI
 760 index for 1850 to 2014. The contour interval is 0.05. The x -axis shows lag years; a positive lag
 761 means dTSI leads SST-NAO. Red and blue shading indicate positive and negative values,
 762 respectively. Areas of darker (lighter) shading indicate statistical significance higher than 90%
 763 (80%). (b) Lagged regression of the January SST-NAO index (contours) against monthly dTSI from
 764 1850 to 2014. The x -axis shows the central years for each of the 41-year running mean calculations
 765 at yearly increments. The y -axis shows lag years. The contour interval is 0.1. Red and blue shading
 766 indicate positive and negative values, respectively. Areas of darker (lighter) shading indicate
 767 statistical significance higher than 90% (80%). The green contours show the same regression for the
 768 value of 0.2, but using the December-January-mean NAO index.

771 4. Discussion

772 We examined the influence of the 11-year solar cycle on the NAO by performing lagged
 773 regression analyses on both recent and historical observations, and on long-term
 774 historical simulation data obtained by using an Earth system model with projected
 775 external forcings. The analyses of observational data showed that a positive NAO signal
 776 develops at the surface in February at around the time of the solar maximum in response
 777 to activity of the PJO that is triggered by anomalous early winter westerly winds at the
 778 subtropical stratopause that are driven by solar radiation in the tropics. Because the
 779 phase of the PJO associated with the positive NAO tends to be reached earlier in winter
 780 as the lag in years increases, the NAO tends to become positive earlier in winter as the
 781 lag in years increases. The relationships of the historical observational data set and the
 782 long-term simulated historical dataset with the NAO were comparable. For the
 783 simulated historical data, the relationships among the subtropical stratopause
 784 temperature, the phases of the PJO and NAO, and the 11-year solar cycle were
 785 reasonable. The analyses of these two data sets also showed that the solar-NAO

786 relationship tended to drift around the mean state on a longer timescale; this drift
787 suggests an oceanic influence on the NAO because the solar-related SST-NAO tends to
788 have a close relation with the NAO of the key month: the SST-NAO tends to lag 2 to 3
789 years relative to the NAO when amplitudes of both indices are sufficiently large.

790

791 In recent years, the solar influence on the winter-mean NAO has been examined
792 in both observational and modeling studies. For example, Gray et al. (2013, 2016) have
793 examined historical SLP data and SSNs for the periods 1870–2010 and 1660–2010,
794 respectively. They found the appearance of the positive peak of the NAO signal to be
795 delayed by a few years relative to the peak solar year. Scaife et al. (2013) performed
796 numerical experiments using the UK Met Office climate model and obtained a similar
797 result, although they performed idealized transient simulations using an amplitude of UV
798 variation that was likely too high. We repeated the same lagged regression analyses for
799 the DJF-mean NAO using recent, historical observations and long-term simulated data,
800 which showed that the peak of the NAO lagged by 0, +1 to +2, and –1 years, respectively
801 (not shown).

802 Thus, the relationship between the solar cycle and winter-mean NAO that we
803 determined disagree with results of Gray et al. (2013, 2016) and Scaife et al. (2013): we
804 obtained a near-zero lag, whereas they obtained positive lags of 3–4 years. However, in
805 our historical analysis of the 194-year (1823–2016) observational dataset, the DJF-mean
806 NAO peak with a lag of +1 to +2 years may represent the influence of lagged response of
807 the SST (Figure 8e). Also it should be noted that for shorter timescales the timing of the
808 peak tended to drift. Similarly, the historical 165-year simulation (1850–2014) also
809 showed an DJF-mean NAO peak at a lag of about –1 year, but the timing of the peak
810 drifted when the dataset was subdivided into shorter periods. This drift would be related
811 to the interaction of the ocean with the NAO. In particular, strength of this interaction
812 with oceanic activity at the surface would have cause the NAO peak to drift from one
813 period to another and prevented us from obtaining a valid estimate of the peak timing,
814 even by using a very long-term dataset.

815 According to the results we obtained from observational data, however, solar-
816 related variations of the NAO index occurred on a sub-seasonal timescale,
817 corresponding with the speed of propagation of the PJO. Therefore, analyses of the
818 NAO at a monthly time scale were necessary to capture the solar–NAO relationship.
819 Without monthly data, an important characteristic of the solar–NAO relationship
820 including the existence of the key month to the top-down mechanism, cannot be
821 detected. Monthly data will also be needed to demonstrate the appearance of a positive

822 NAO signal earlier in winter with increasing years after peak solar activity. Sub-
823 seasonal variations of the solar-related SST-NAO (Figures 8e, 13a) suggest that
824 enhancement of the solar-related NAO at a few years lag of early winter is a direct
825 result of the SST response, and the lagged response of SST is a result of the thermal
826 inertia of the ocean. On the other hand, the enhanced solar-related SST signal in early
827 winter (Figures 6, 10b) is a response to the tendency of the NAO to be more strongly
828 affected by SST during early winter (Czaja and Frankignoul, 2002).

829

830 However, even if monthly data were available, 50-year-scale fluctuations of the
831 timing of the peak NAO signals at key times (e.g., February of lag 0 years) would prevent
832 statistically valid capture of the interaction of the solar-NAO signal with oceanic
833 dynamics. Thus, the solar-related NAO signal cannot be captured by a simple spectral
834 analysis method such as that of Chiodo et al. (2019). In fact, the solar-related NAO signal
835 tends to be more prominent only during specific months (e.g., February), and even if a
836 specific month is chosen for analysis, the NAO peak of that month may also drift at a 50-
837 year scale. Therefore, the spectral structure of the solar-related NAO signal will be very
838 complex. Development of a new method designed specifically to capture the solar-related
839 signal from such complex data is needed.

840 To examine more directly the effect of the solar cycle on long-term ocean
841 dynamics, we used the SST-NAO derived from monthly observation data (Figure 8e and
842 8f) to show that the SST-NAO signal was sometimes in phase with the solar cycle with a
843 positive lag of 2 to 3 years, similar to the NAO signal in February. During these periods,
844 both signals tended to be amplified, thus suggesting them to be strongly coupled.
845 Although the periods when the SST-NAO was in phase with the solar cycle were not very
846 long, the February NAO and the SST-NAO indices tended to be well correlated
847 throughout the period 1854–2016. Thus, because the winter SST-NAO and February-
848 NAO tended to be closely related when the SST-NAO signal was in phase with the solar
849 cycle, we suggest that the February NAO signal tended to drive SST, and this forcing
850 interacted with decadal oceanic dynamics to create an SST signal in phase with the solar
851 cycle (Kodera et al., 2016) and amplified both the SST-NAO and NAO signals. The
852 results of our simulations also support this mechanism.

853 To more directly assess the relationship between the solar cycle and the decadal
854 component of the NAO, we compared the time series of the solar cycle and decadal
855 components of the February-mean NAO index obtained from observed data (Figure 14a)
856 or the December–January mean of the NAO index obtained from simulated data (Figure
857 14b). The decadal component of the NAO index was calculated by treating these monthly

858 mean values as annual values and filtering to extract frequencies from 8 to 15 years using
859 the Lanczos band-pass filter with a window width of 31 years (Hamming, 1977).
860 Comparison of the SSN with the decadal NAO from the observational data (Figure 14a)
861 showed that the maxima and minima of the solar cycles were almost synchronous
862 throughout the period analyzed, although there was some phase drift between cycles. The
863 peaks matched reasonably well around years 1850, 1860, 1885, 1905, 1925, 1938, 1980,
864 1990, 2000, and 2010. The 41-year running correlations between SSN and decadal NAO
865 were positive throughout the period analyzed. In contrast, the decadal component of the
866 SST-NAO at a lag of 2 years correlated well with SSN only for limited periods of time
867 (Figure 8f). This synchronicity of the decadal component of the NAO with the solar cycle
868 likely represents a nonlinear response of the ocean, as pointed out by Thiéblemont et al.
869 (2015).

870 Comparison of the TSI and decadal NAO from simulated data (Figure 14b) also
871 showed good synchronicity throughout the period analyzed, with peaks matching
872 reasonably well around years 1860, 1870, 1885, 1895, 1905, 1918, 1970, 1990, and 2000,
873 although the match was poor around 1940. The 41-year running correlations between the
874 TSI and decadal NAO were positive throughout. It should be noted that the solar
875 synchronous component of the NAO was extracted from annual data, which means that
876 the component was completely annually locked and reflected forcing of the PJO. Thus,
877 both top-down and oceanic mechanisms appeared to be active in the solar-NAO system.

878 Thus, synchronicities of the solar cycle and the decadal component of the NAO
879 occur only when signals of specific months are selected, which suggests that the
880 monthly solar signal tends to be locked, but the signal is nearly synchronized with the
881 NAO when considered decadal. This is an interesting phenomenon. Though Chiodo et
882 al. (2019) claims the solar signal since the mid-1960s is a chance occurrence due to
883 internal variability, it will not, if we look at Figure 14a.

884
885
886
887
888
889
890
891
892
893

894
895
896
897
898
899
900
901
902
903
904
905
906
907
908
909
910
911
912
913
914
915
916
917
918
919
920
921
922
923
924
925
926
927
928
929

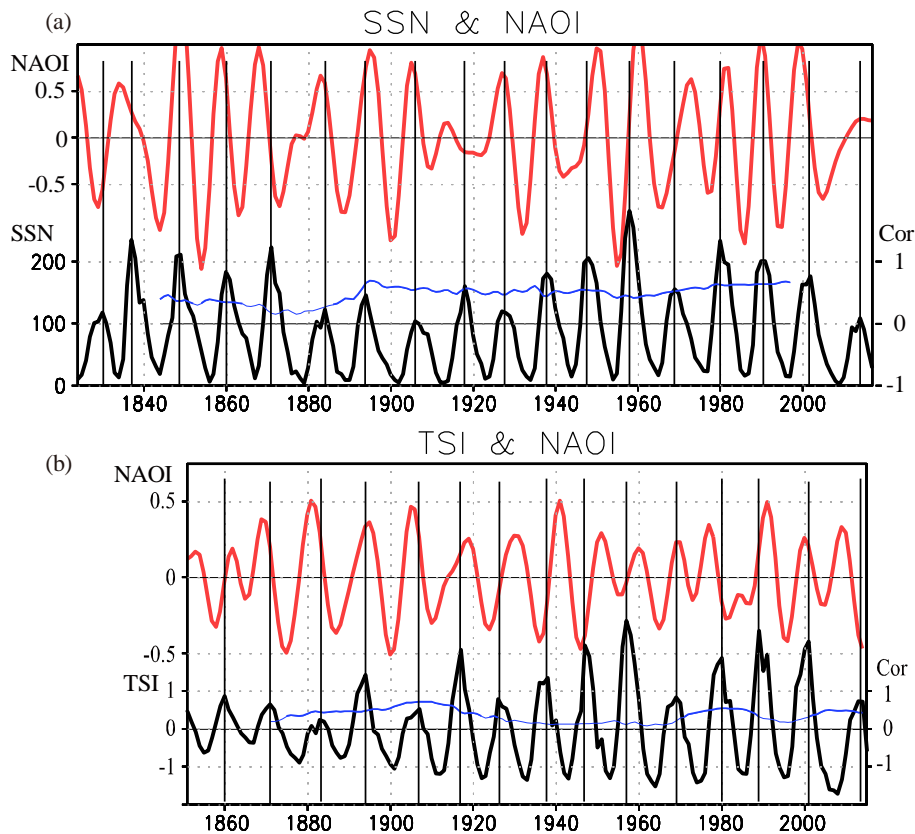


Figure 14. Comparison of observed and simulated NAO index and solar indices. (a) Decadal component of the February-mean NAO index (red line) and SSN from observation data. Peaks of SSN are marked by vertical black lines. Forty-one-year running correlations between NAO index and SSN are shown by the blue line with the right label. Correlation greater than 95% significance level is shown by thick line. (b) Same as (a) but for simulated DJ mean NAO index (red line) and TSI. Running correlations of TSI are again shown by blue line. On both panels, vertical lines mark solar maxima.

Neither the solar signal of the NAO (Figure 12a) nor the synchronicity of the decadal NAO and the solar cycle (Figure 14b) are as strongly evident in our simulation results as they are in the observational data. Moreover, the period covered by our simulation is relatively short, so it may be better to regard our simulation results as some reference in the present. Although our simulation results had some features in common with the observed solar–NAO relationship, it may be possible to derive more congruence by running historical simulations over longer time intervals. Future analyses incorporating more historical simulations (e.g., CMIP6 simulations) or performing ensemble runs will be useful in this regard.

930 **5. Conclusions**

931 The results of our analysis suggest that the solar–NAO relationship is created
932 by a top-down mechanism modulated by the ocean. A possible effect of the ocean is
933 evident in our monthly mapping of the time of appearance in winter of the NAO, which
934 showed that the NAO tended to appear earlier in winter as the lag in years increased. If
935 formation of the NAO were entirely a top-down mechanism, there would be no
936 asymmetry between positive- and negative-lag years. The agent of this asymmetry will
937 be the thermal inertia of the ocean. Another indication of an oceanic effect is the drift
938 we identified of the timing of the peak NAO relative to solar maximum years on a 50-
939 year timescale. This drift suggested the existence of a strong nonlinear interaction
940 between the solar cycle and ocean dynamics. The modulation of the decadal component
941 of the NAO also suggested such an interaction. The direct relationship between the solar
942 cycle and ocean dynamics requires further examination.

943

944 **Acknowledgments**

945 This research was supported in part by Grants-in-Aid for Scientific Research
946 (26287115, 26281016, 16H01184, 18H01280) from the Ministry of Education, Culture,
947 Sports, Science and Technology of Japan. The ERA-Interim data is available from the
948 ECMWF website ([https://www.ecmwf.int/en/forecasts/datasets/reanalysis-datasets/era-](https://www.ecmwf.int/en/forecasts/datasets/reanalysis-datasets/era-interim)
949 [interim](https://www.ecmwf.int/en/forecasts/datasets/reanalysis-datasets/era-interim)). Monthly data of the F10.7 index are available from the Natural Resources
950 Canada website (<https://www.spaceweather.gc.ca/solarflux/sx-5-en.php>). The sources of
951 satellite data sets are <https://rda.ucar.edu/datasets/ds067.1/>,
952 <https://rda.ucar.edu/datasets/ds067.3/>, and <https://rda.ucar.edu/datasets/ds067.4/> for the
953 NCEP/CPC, and <https://aura.gsfc.nasa.gov/science/data.html> for the Aura-MLS.
954 Historical NAO index was obtained from the University of East Anglia Climate
955 Research Unit, UK website (<https://crudata.uea.ac.uk/~timo/datapages/naoi.htm>).
956 Historical sun spot numbers were obtained from the Royal Observatory of Belgium
957 website (<http://www.sidc.be/silso/datafiles>). Historical SST data was obtained from the
958 NOAA website ([https://www.ncdc.noaa.gov/data-access/marineocean-data/extended-](https://www.ncdc.noaa.gov/data-access/marineocean-data/extended-reconstructed-sea-surface-temperature-ersst-v5)
959 [reconstructed-sea-surface-temperature-ersst-v5](https://www.ncdc.noaa.gov/data-access/marineocean-data/extended-reconstructed-sea-surface-temperature-ersst-v5)). The numerical data used in this study
960 are available from [https://climate.mri-jma.go.jp/pub/archives/Kuroda-et-](https://climate.mri-jma.go.jp/pub/archives/Kuroda-et-al_Solar_NAO_MRI-ESM2.0)
961 [al_Solar_NAO_MRI-ESM2.0](https://climate.mri-jma.go.jp/pub/archives/Kuroda-et-al_Solar_NAO_MRI-ESM2.0).

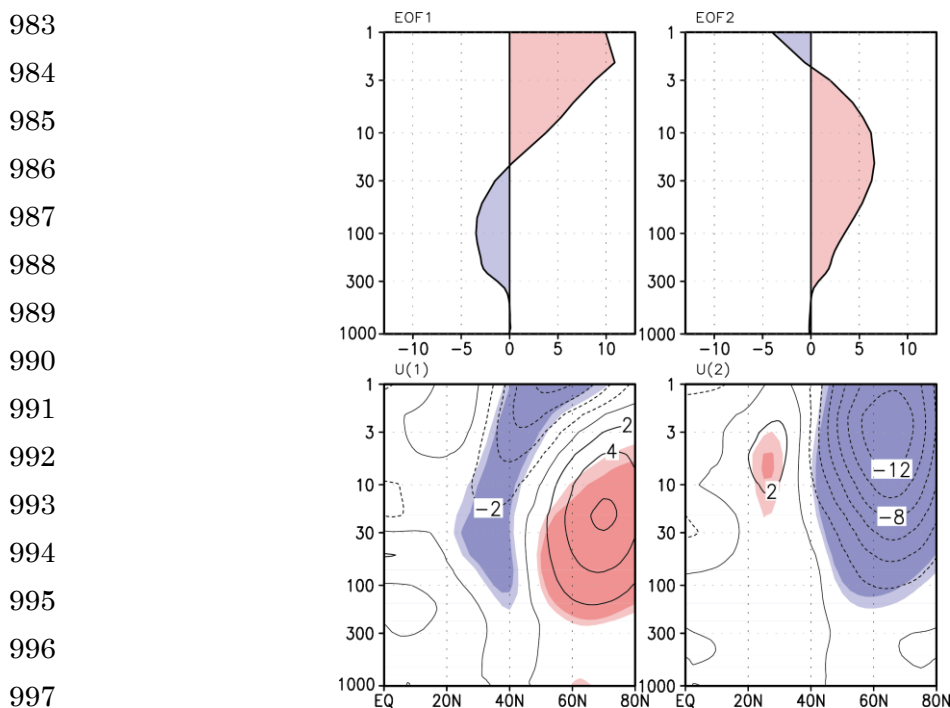
962

963 **Appendix A**

964 Following Kuroda and Kodera (2004), we defined the Polar-night Jet

965 Oscillation (PJO) and its index by the two leading empirical orthogonal functions
 966 (EOFs) and their principal component (PC) time series of anomalous polar temperatures
 967 from 1000 to 1 hPa levels during extended winter (November to April) by using ERA-
 968 Interim data (Figure A1, top panels). Almost 90% of the variance in polar temperatures
 969 was explained by these two EOFs. For calculation of EOFs, the physical thickness
 970 (meters) of each pressure level was considered, and polar temperature was defined as
 971 the monthly average temperature poleward of 80°N. Because the amplitude of the PJO
 972 signal in the troposphere is negligible, the PJO is a result of mostly stratospheric
 973 variability.

974 We also calculated the regression of zonal-mean zonal wind against each PC
 975 time series (Figure A1, lower panels). The state vector tended to rotate counterclockwise
 976 with time when represented in two-dimensional space (PJO-space) represented by the
 977 principal component 1 (PC1) (x -axis) and PC2 (y -axis). This counterclockwise rotation
 978 of the state vector corresponds to the poleward and downward shift of the anomalous
 979 zonal-mean zonal wind with time, which Kuroda and Kodera (2001) have defined as the
 980 temporal evolution of the PJO. Correlation of PC1 (PC2) with the NAO index is 0.28 (–
 981 0.15) if all 6×38 months are used, and both indices are then related to the NAO index
 982 at greater than 99% statistical significance.



983
 984
 985
 986
 987
 988
 989
 990
 991
 992
 993
 994
 995
 996
 997
 998 **Figure A1.** Upper panels: Vertical profiles of the EOF1 (left) and EOF2 (right) of anomalous
 999 northern winter polar cap temperatures. Lower panels: Regressions of time series of zonal-mean
 1000 zonal winds against the EOF1 (left) and EOF2 (right). The y -axes are height (hPa). The x -axes of

1001 upper panels are temperature (K), those of lower panels are latitude. Dark (light) shading (red
1002 positive, blue negative) indicates areas of greater than 99% (95%) statistical significance.

1003

1004 **References**

1005 Andrews, D. G., J. R. Holton, and C. B. Leovy (1987), *Middle Atmosphere Dynamics*
1006 (489 pp.), Orlando: Academic Press.

1007 Andrews, M. B., Knight, J. R., & Gray L. J. (2015). A simulated lagged response of the
1008 North Atlantic Oscillation to the solar cycle over the period 1960-2009. *Environmental*
1009 *Research Letters*, *10*, 1–10. <https://doi.org/10.1088/1748-9326/10/5/054022>

1010 Bailey, S. M, C. A. Barth, and S. C. Solomon (2002), A model of nitric oxide in the lower
1011 thermosphere, *Journal of Geophysical Research: Atmospheres*, *107*(A8), 1205,
1012 <https://doi.org/10.1029/2001JA000258>.

1013 Chiodo, G. et al. (2016), The impact of a future solar minimum on climate change
1014 projection in the northern hemisphere. *Environmental Research Letters*, *11*, 034015.
1015 <https://doi.org/10.1088/1748-9326/11/3/034015>.

1016 Chiodo, G., Oehrlein, J., Polvani, L. M., Fyfe, J. C., & Smith A. K. (2019), Insignificant
1017 influence of the 11-year solar cycle on the North Atlantic Oscillation. *Nature*
1018 *Geoscience* *12*, 94–99. <https://doi.org/10.1038/s41561-018-2293-3>

1019 Czaja, A. and C. Frankignoul (2002), Observed impact of Atlantic SST anomalies on the
1020 North Atlantic Oscillation, *J. Clim.*, *15*, 606-623, [https://doi.org/10.1175/1520-0442\(2002\)015<0606:OIOASA>2.0.C;2](https://doi.org/10.1175/1520-0442(2002)015<0606:OIOASA>2.0.C;2).

1022 Dee, D. P. et al. (2011), The ERA-Interim reanalysis: configuration and performance of
1023 the data assimilation system, *Quarterly Journal of the Royal Meteorological Society*,
1024 *137*, 553–597, <https://doi.org/doi:10.1002/qj.828>.

1025 Dhomse, S.S., et al. (2016), On the ambiguous nature of the 11 year solar cycle signal in
1026 upper stratosphere ozone. *Geophysical Research Letters*, 43, 7241-7249, [https://](https://doi.org/doi:10.1002/2016GL069958)
1027 doi.org/doi:10.1002/2016GL069958.

1028 Eyring, V. et al. (2016), Overview of the Coupled Model Intercomparison Project Phase
1029 6 (CMIP6) experimental design and organization, *Geoscientific Model Development*,
1030 9, 1939-1958, <https://doi.org/doi:10.5194/gmd-9-1937-2016>.

1031 Gray, L. J. et al. (2010), Solar influence on climate, *Review of Geophysics*, 48, RG4001,
1032 <https://doi.org/doi:10.1029/2009RG000282>.

1033 Gray, L. J. et al., (2013), A lagged response to the 11 year solar cycle in observed winter
1034 Atlantic/European weather patterns, *Journal of Geophysical Research: Atmospheres*,
1035 108, 13,405-13,420, <https://doi.org/doi:10.1029/2013JD020062>.

1036 Gray, L. J., T. J. Woollings, M. Andrews, and J. Knight, (2016), Eleven-year solar cycle
1037 signal in the NAO and Atlantic / European blocking, *Quarterly Journal of the Royal*
1038 *Meteorological Society*, 142, 1890-1903, <https://doi.org/doi:10.1002/1j.2782>.

1039 Hamming, R. W. (1977), *Digital Filters*, pp. 296, Prentice Hall, Englewood Cliffs, N.J.

1040 Hines, C. O., (1997), Doppler-spread parameterization of gravity-wave momentum
1041 deposition in the middle atmosphere. 2. Broad and quasi-monochromatic spectra, and
1042 implementation, *Journal of Atmospheric and Solar-Terrestrial Physics*, 59, 387-400.

1043 Huang, B., et al., (2017), Extended Reconstructed Sea Surface Temperature, Version 5
1044 (ERSSTv5): Upgrades, Validations, and Intercomparisons.

1045 Hurrell, J. W., Y. Kushnir, G. Ottersen, and M. Visbeck, (edit) (2003), *The North Atlantic*
1046 *Oscillation*, Geophysical Monographs, vol. 134, pp. 279, American Geophysical
1047 Union, Washington, DC.

1048 Ineson, S., A. A. Scaife, J. R. Knight, J. C. Manners, N. J. Dunstone, L. J. Gray, and J. D.

1049 Haigh (2011), Solar forcing of winter climate variability in the northern hemisphere,
1050 *Nature Geoscience*, 4, 753-757, <https://doi.org/doi:10.1038/NGEO1282>.

1051 Jones, P.D., T. Jonsson, and D. Wheeler (1997), Extension to the North Atlantic
1052 Oscillation using early instrumental pressure observations from Gibraltar and South-
1053 West Iceland, *Int. J. Climatol.* 17, 1433-1450. [https://doi.org/doi:10.1002/\(SICI\)1097-
1054 0088\(19971115\)17:13<1433::AID-JOC203>3.0.CO;2-P](https://doi.org/doi:10.1002/(SICI)1097-0088(19971115)17:13<1433::AID-JOC203>3.0.CO;2-P).

1055 Kodera, K. (1995), On the origin and nature of the interannual variability of the winter
1056 stratospheric circulation in the northern hemisphere, *Journal of Geophysical Research:*
1057 *Atmospheres*, 1070(D7), 14,077-14,087, <https://doi.org/doi:10.1029/95JD01172>.

1058 Kodera, K., and Y. Kuroda, (2002), Dynamical response to the solar cycle, *Journal of*
1059 *Geophysical Research: Atmospheres*, 107(D24), 4749,
1060 <https://doi.org/doi:10.1029/2002JD002224>.

1061 Kodera, K., R. Thiéblemont, S. Yukimoto, and K. Matthes (2016), How can we
1062 understand the global distribution of the solar cycle signal on the Earth's surface?
1063 *Atmos. Chem. Phys.*, 16, 12925-12944, <https://doi.org/10.5194/acp-16-12925-2016>.

1064 Kopp, G. and J. L. Lean (2011), A new, lower value of total solar irradiance: Evidence
1065 and climate significance, *Geophysical Research Letters*, 38, L01706,
1066 <https://doi.org/doi:10.1029/2010GL045777>.

1067 Kuroda, Y., and K. Kodera (2001), Variability of Polar-night jet in the northern and
1068 southern hemispheres, *Journal of Geophysical Research: Atmospheres*, 106 (D18), 20,
1069 703-20, 713, <https://doi.org/10.1029/2001JD900226>.

1070 Kuroda, Y., and K. Kodera (2002), Effect of solar activity on the polar-night jet oscillation
1071 in the northern and southern hemisphere winter, *Journal of the Meteorological Society*
1072 *of Japan*, 80, 973-984, <https://doi.org/10.2151/jmsj.80.973>.

1073 Kuroda, Y., and K. Kodera (2004), Role of the polar-night jet oscillation on the formation
1074 of the Arctic Oscillation in the northern hemisphere winter, *Journal of Geophysical*
1075 *Research: Atmospheres*, *109*, D11112, <https://doi.org/doi:10.1029/2003JD004123>.

1076 Lean, L. et al., (1997), Detection and parameterization of variations in solar mid and near-
1077 ultraviolet radiation (200-400 nm). *Journal of Geophysical Research: Atmospheres*,
1078 *102 (D25)*, 29, 939-29, 956, <https://doi.org/10.1029/97JD02092>.

1079 Ma, H., H. Chen, L. Gray, L. Zhou, X. Li, R. Wang, and S. Zhu, (2018), Changing
1080 response of the North Atlantic/European winter climate to the 11 year solar cycle,
1081 *Environmental Research Letters*, *13*, 034007, [https://doi.org/10.1088/1748-](https://doi.org/10.1088/1748-9326/aa9e94)
1082 [9326/aa9e94](https://doi.org/10.1088/1748-9326/aa9e94).

1083 Maisel, L. (1971), *Probability, statistics and random processes*, (280pp.) New York,
1084 Simon & Schuster, Inc.

1085 Matthes, K., U. Langematz, L. Gray, K. Kodera, and Labitzke, K. (2004), Improve 11-
1086 year solar signal in the Freie Universitaet Berlin Climate middle atmosphere Model
1087 (FUB-CMAM), *Journal of Geophysical Research: Atmospheres*, D06101,
1088 <https://doi.org/doi:10.1029/2003JD004012>.

1089 Matthes, K., Y. Kuroda, K. Kodera, and U. Langematz, (2006), Transfer of the solar signal
1090 from the stratosphere to the troposphere: Northern winter, *Journal of Geophysical*
1091 *Research: Atmospheres*, *111*, D06108, <https://doi.org/doi:10.1029/2005JD006283>.

1092 Matthes, K. et al. (2017), Solar forcing for CMIP6 (v3.2), *Geoscientific Model*
1093 *Development Discussions, Copernicus Publications*, *10 (6)*, 2247-2302,
1094 <https://doi.org/doi:10.5194/gmd-10-2247-2017>.

1095 Meehl, G. A., J. M. Arblaster, K. Matthes, F. Sassi, H. van Loon (2009), Amplifying the
1096 Pacific climate system response to a small 11-year solar cycle forcing, *Science*, *325*,

1097 1114-1118, <https://doi.org/doi:10.1126/science.1172872>.

1098 Misios S. et al. (2019), Slowdown of the walker circulation at solar cycle maximum,
1099 PNAS, 116, 7186-7191, <https://doi:10.1073/pnas.1815060116>.

1100 Mitchell D. M. et al. (2015), Solar signals in CMIP-5 simulations: the stratospheric
1101 pathway, *Q. J. R. Meteorol. Soc.*, 141, 2390-2403, <https://doi.org/doi:10.1002/qj.2530>.

1102 Scaife, A. A., S. Ineson, J. R. Knight, L. Gray, K. Kodera, and D. M. Smith, A mechanism
1103 for lagged North Atlantic climate response to solar variability (2013), *Geophysical*
1104 *Research Letters*, 40, 434-439, <https://doi.org/doi:10.1002/grl.50099>.

1105 Schwartz, M. J. et al. (2008), Validation of the Aura microwave limb sounder temperature
1106 and geopotential height measurements, *Journal of Geophysical Research:*
1107 *Atmospheres*, 103, D15S11, <https://doi.org/doi:10.1029/2007JD008783>.

1108 Spiegl, T., and U. Langematz (2020), Twenty-first-century climate hot spots in the light
1109 of a weakening sun, *Journal of Climate* 33, 3431-3447, [https://doi.org/10.1175/JCLI-](https://doi.org/10.1175/JCLI-D-19-0059.1)
1110 [D-19-0059.1](https://doi.org/10.1175/JCLI-D-19-0059.1)

1111 Thiéblemont, R., K. Matthes, N-E. Omirani, K. Kodera, and F. Hansen (2015), Solar
1112 forcing synchronized decadal North Atlantic climate variability, *Nature*
1113 *Communications*, 6:8268, <https://doi.org/doi:10.1038/ncomms9268>.

1114 Yukimoto, S., et al. (2012), A new Global Climate Model of the Meteorological Research
1115 Institute: MRI-CGCM3 -Model description and basic performance, *Journal of the*
1116 *Meteorological Society of Japan*, 90A, 23-64, <http://doi.org/10.2151/jmsj.2012-A02>.

1117 Yukimoto, S., et al. (2019), The MRI Earth System Model version 2.0, MRI-ESM2.0:
1118 Description and basic evaluation of the physical component, *Journal of the*
1119 *Meteorological Society of Japan*, 97, 931-965, <http://doi.org/10.2151/jmsj.2019-051>.

1120